

Exploring Topological Boundary Effects through Quantum Trajectories in Dissipative SSH Models

Giulia Salatino ,¹ Gianluca Passarelli ,² Angelo Russomanno ,² Giuseppe E. Santoro,^{3, 4} Procolo Lucignano ,² and Rosario Fazio ,^{4, 2}

¹*Scuola Superiore Meridionale, Via Mezzocannone, 4 80138, Napoli, Italy.*

²*Dipartimento di Fisica E. Pancini, Università di Napoli Federico II, Complesso di Monte S. Angelo, via Cinthia, I-80126 Napoli, Italy.*

³*SISSA, Via Bonomea 265, I-34136 Trieste, Italy.*

⁴*International Centre for Theoretical Physics, P.O.Box 586, I-34014 Trieste, Italy.*

(Dated: November 11, 2024)

We investigate the topological properties of the Su-Schrieffer-Heeger (SSH) model under dissipative dynamics using the quantum trajectory approach. Our study explores the preservation or breakdown of topological edge states, particularly focusing on the effects of symmetry-preserving and symmetry-breaking dissipations. We employ the Disconnected Entanglement Entropy (DEE) as a marker for detecting topological phases in the system, which is subjected to Lindblad dynamics. The analysis reveals that, while dissipation in the bulk minimally affects the system's topological features, dissipation at the boundary leads to the destabilization of the edge modes, independently of the symmetry properties of the dissipation.

I. INTRODUCTION

Condensed matter physics has seen significant advancements through the investigation of systems characterized by non-trivial topological phases [1]. While much attention has traditionally focused on the ground state properties of both free and interacting many-body systems, recent research has expanded our understanding of topological systems to include non-Hermitian [2, 3] and open quantum systems governed by Lindblad dynamics [4–7].

The interplay between topology and dissipation gives rise to novel phases and dynamics not observed in closed systems, such as the breakdown of bulk-boundary correspondence and the emergence of the non-Hermitian skin effect [2].

Symmetries play a crucial role in determining the topological properties of these systems. The tenfold way classification, based on Altland-Zirnbauer (AZ) classes, categorizes topological phases that can appear in the ground state of closed systems [8]. However, in open systems, new classifications have been proposed. Topological phases in non-Hermitian systems have been explored in [9, 10]. Symmetries in Lindbladians have also been investigated [11–14]. Altland et al. [7] extended the tenfold classification to open fermionic systems described by the Lindblad equation. Cooper et al. [6] extended this framework to open systems characterized by quadratic Lindblad superoperators, accounting for the symmetries of both coherent and dissipative contributions, focusing on the impact of these symmetries on the Lindbladian spectrum. Kawasaki et al. recently expanded this classification by introducing the shifted sublattice symmetry class [15].

Defining a suitable topological invariant for open topological insulators remains an open challenge. Several quantities have been proposed, including non-Hermitian

topological invariants [16–18], the Uhlmann phase [19–21], the Ensemble Geometric phase [22, 23], and the recent mixed-state topological order parameter introduced by Huang and Diehl [24].

In this work, we aim to explore the topological properties of free fermion Lindbladian systems by combining insights from unitary systems with the unraveling of Lindblad dynamics along quantum trajectories. For this purpose, we will employ the Disconnected Entanglement Entropy (DEE), initially introduced in [25]. DEE is a robust measure of symmetry-protected topological phases in contexts where traditional entanglement measures, such as the von Neumann entropy, fall short [26–30]. Unlike the winding number, the DEE is not a bulk topological invariant. Instead, it quantifies the entanglement between topological edge states by partitioning the system into disjoint regions and measuring the entropy of the reduced density matrix for these regions. It remains robust under local, unitary, and symmetry-preserving quench dynamics, as shown for both the SSH chain and the Kitaev wire [31, 32]. A recent study confirmed its effectiveness as a topological marker for a periodically driven Kitaev chain [33]. Additionally, it has been demonstrated that the DEE can detect long-range entanglement in certain phases that are not symmetry-protected topological phases [34], as well as Majorana zero modes in semiconductor-superconductor heterostructures [35]. This order parameter, closely related to entanglement entropy, is also experimentally accessible, as discussed in [36–38].

We investigate a paradigmatic case in this context — the Su-Schrieffer-Heeger (SSH) model, well-known for its simplicity and the rich variety of phenomena it presents. Initially proposed to describe electron behavior in polyacetylene [39, 40], it serves as a one-dimensional example of a system with topological edge states protected by chiral symmetry [41, 42]. Specifically, we examine the

DEE of an SSH chain under different types of dissipation, classified according to the generalized tenfold way in Ref. [6]. Beyond exploring different symmetry classes, we also consider distinct dissipation ranges, distinguishing between *global* dissipation, which acts across the entire chain, and *central* dissipation, which affects only a central portion, leaving the edges untouched. Our results show that while bulk dissipation minimally impacts the system's topological features, boundary dissipation destabilizes the edge modes. This study provides new insights into the interplay between topology and dissipation, revealing the critical role of the spatial location of dissipation on the persistence in time of an initial topological state. In some sense we generalize the results of [32]. There it was shown that an initial doublet of entangled topological modes persisted for a time linear in the system size, when the evolution occurred under a local (trivial or topological) Hamiltonian. Here we extend this result to quadratic dissipators, and see that the topological mode persists for a time linear in the system size if the dissipator does not affect the boundary, independently of its symmetry properties.

This work is structured as follows: In [Section II](#), we review the SSH model and its topological properties, introduce the types of dissipative dynamics we will examine, describe the quantum jump unraveling of the Lindblad equation, and outline our methodology for calculating the DEE. In [Section III](#), we present the DEE and the method to calculate its time evolution. In [Section IV](#), we discuss our main results, including the effects of different dissipative dynamics on the edge modes characterizing the system's initial topological phase. We also explore the time evolution of the DEE and the scaling behavior of a DEE-related quantity: the time at which the DEE deviates from its quantized initial value due to dissipation. Lastly, we conduct a statistical analysis of the DEE's variation after a quantum jump, considering both the timing and location of the jump for a comprehensive time- and index-resolved analysis. In [Section V](#), we discuss the implications of our findings for the understanding of dissipation in topological phases and propose potential directions for future research.

II. THE MODEL

We consider a dissipative dynamics described by the master equation for the density matrix $\hat{\rho}(t)$ in the Lindblad form [43, 44] ($\hbar = 1$)

$$\frac{d}{dt}\hat{\rho}(t) = -i[\hat{H}_{\text{SSH}}, \hat{\rho}(t)] + \sum_{\mu} \left(\hat{L}_{\mu} \hat{\rho}(t) \hat{L}_{\mu}^{\dagger} - \frac{1}{2} \{ \hat{L}_{\mu}^{\dagger} \hat{L}_{\mu}, \hat{\rho}(t) \} \right), \quad (1)$$

where \hat{H}_{SSH} is the Hamiltonian of the SSH model [39, 40] and the Lindblad operators \hat{L}_{μ} characterize the dissipative dynamics.

The SSH model describes a 1D atomic chain with two atoms per unit cell, on which electrons hop with staggered hopping amplitude [45]. Its Hamiltonian, with open boundary conditions, is

$$\hat{H}_{\text{SSH}} = -J_o \sum_{j=1}^N \hat{c}_{j,A}^{\dagger} \hat{c}_{j,B} - J_e \sum_{j=1}^{N-1} (\hat{c}_{j+1,A}^{\dagger} \hat{c}_{j,B} + \text{h.c.}), \quad (2)$$

where $J_o, J_e > 0$, A and B indicate the type of atom within the unit cell (the sublattice index), N is the number of unit cells and $L = 2N$ is the number of sites in the chain.

The first (second) dissipation satisfies (breaks) the generalized symmetry relations that characterize the BDI class in presence of dissipation, as proposed in Ref. [6]. Further details about this dissipative tenfold way are provided in [Appendix B](#). At half filling, the ground state of \hat{H}_{SSH} displays two distinct topological phases. When $J_o/J_e > 1$ the phase is topologically trivial, while it is topological for $J_o/J_e < 1$.

In the topological phase, the density profile of each edge shows one localized fermion on the left end and one on the right end of the chain – see sketch in [Fig. 1](#) [Appendix A](#) for further details and Ref. [45, 46]. This is related to the fact that, in this topological fully-dimerized limit, one fermion is localized on each inter-cell link, and two unpaired fermions are left on the extreme sites. In the thermodynamic limit these topological boundary excitations are degenerate and are at zero energy. For any finite size they hybridize, and an exponentially small gap open between the even and the odd superposition of them.

Therefore at finite size, half filling and zero temperature – when all the lower band is occupied – only the even superposition $\frac{1}{\sqrt{2}} (\hat{c}_{N,B}^{\dagger} + \hat{c}_{1,A}^{\dagger})$ of the topological boundary modes is occupied, while the odd is empty.

This even superposition of boundary modes can be written as a Bell state, as it is explained in detail in [Appendix A](#) and is such that the two distant edges are entangled. This is the only long-range entanglement of the whole chain that can be detected when the system is in a topological phase [32]. Beyond it there is only short-range entanglement across each intercell link.

The Hamiltonian of the SSH model (2) falls in the BDI symmetry class of the AZ tenfold way [8], which leads to a \mathbb{Z} type of topological invariant in 1D. This means that the edge states are protected by time-reversal, chiral and particle-hole symmetries and that there is an infinite countable number of distinct topological phases with the symmetries preserved (see also [Appendix B](#)). In the presence of periodic boundary conditions (PBC) translation symmetry allows to detect the topological phase using non-local topological invariants like the winding number or Zak phase in k space [47, 48].

In this manuscript we focus instead on OBC, consider two different Lindbladians operators and study the dynamics of the system in the two cases. In order to define them, let us state that the sum over μ in Eq. (1) runs

over two channels of type (j, A) and (j, B) , j being the cell index. The first type of Lindbladian we consider is the global Symmetry-Preserving Dissipation (SPD) dynamics [6], for which the jump operators are defined as:

$$\begin{cases} \hat{L}_{j,A} = \sqrt{\gamma} \hat{c}_{j,A}, \\ \hat{L}_{j,B} = \sqrt{\gamma} \hat{c}_{j,B}^\dagger, \end{cases} \quad (3)$$

and act on all the cells of the chain (global dissipation). The non-Hermitian Hamiltonian associated to this dynamics has been first theoretically proposed in Ref. [49] and then experimentally implemented [50] in a photonic lattice with engineered gain and loss, and robust topological edge states have been observed. We sketch this dissipation in Fig. 1(b) emphasizing that in each cell there is one site where fermions are injected by the Lindbladian, and the other where fermions are sucked, with the same rate.

The second Lindbladian is the global Symmetry-Breaking Dissipation (SBD) [6], and its jump operators are

$$\begin{cases} \hat{L}_{j,A} = \sqrt{\gamma} \left(\hat{c}_{j,A} + e^{i\theta} \hat{c}_{j,B} \right), \\ \hat{L}_{j,B} = \sqrt{\gamma} \left(\hat{c}_{j,B} + e^{i\theta} \hat{c}_{j+1,A} \right). \end{cases} \quad (4)$$

We sketch this dissipation in Fig. 1(c) and emphasize that each Lindblad operator acts on a couple of sites and has the effect of sucking away fermions from the system. The first (second) dissipation satisfies (breaks) the generalized symmetry relations that characterize the BDI class in presence of dissipation, as proposed in Ref. [6]. Further details about this topological classification of dissipators (the so-called dissipative tenfold way) are provided in Appendix B.

In order to assess the impact of dissipation on the edge modes, we will consider the possibility that the jump operators involve only a portion of αL central sites, with $\alpha \in [0, 1]$ such that, once we fix the parameters of the system and the range of lengths we will deal with, the edges of the chain are left untouched. This can be achieved by adjusting the site-dependent values of $\gamma_{j,A/B}$ so that they are different from zero on a limited portion of central sites. For this reason, we will refer to the latter as the central α -SPD or α -SBD dynamics depending on the type of jump operators that will be considered. We have numerically verified that choosing $\alpha = 0.8$ is sufficient to separate the bulk dissipation from the boundary.

We remark again that Fig. 1(a) is a sketch representing how the zero-energy modes are exponentially localized on the edges of the chain in such a way that a central α -SPD or α -SBD environment with a suitable choice of α might not touch them. Fig. 1(b) helps visualizing the action of the Lindblad operators of the global SPD environment. By suitably turning off and on gain and loss along the chain through α , this becomes the central α -SPD dissipa-

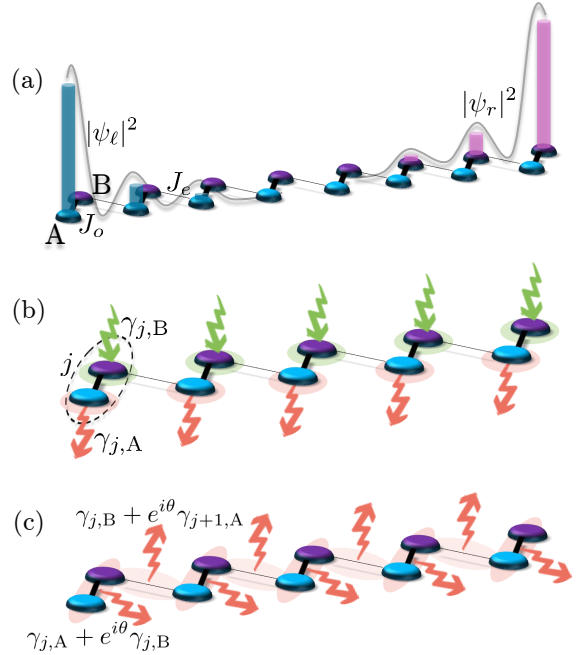


FIG. 1: (a) Sketch of the probability amplitude of the zero-mode states $|\psi_\ell\rangle$ and $|\psi_r\rangle$ that are exponentially localized on the edges of the SSH chain. (b) Sketch of the symmetry-preserving environment. The dotted oval represents the j -th unit cell. The green and orange shaded shapes represent the sites involved by the single Lindblad operators. (c) Sketch of the symmetry-breaking environment.

pation. Fig. 1(c) is a similar sketch for the global SBD dynamics.

The Lindbladian that we take into account is quadratic, since the Hamiltonian of the SSH model is quadratic and the considered jump operators are linear in the fermionic operators. Given a Gaussian state as initial condition of a quadratic dissipative dynamics, its Gaussianity is preserved in time, so that Wick's theorem holds for its whole evolution in time (see Appendix C for more details on Gaussian states). Furthermore, for quadratic Lindbladians the tenfold symmetry classification of Cooper et al. [6] holds.

II.1. Quantum jump unraveling of the Lindblad equation

In the following, we study the dynamics of our open system via the quantum trajectory approach [44, 51–54].

In the quantum trajectory approach, the dynamics under the action of the environment is described as an average over many realizations of a non-Hermitian Hamiltonian dynamics with classical noise. Each realization of this stochastic process is a quantum trajectory and the ensemble evolution provided by the Lindblad equation

(1) is obtained by averaging over infinite trajectories (in the practice, over a finite number of trajectories with an errorbar provided by the fluctuation around the average.) The stochastic noise acting on each trajectory can be seen as a result of measurements made by the environment.

In this paper we focus on a specific type of quantum-trajectory approach, the so-called quantum-jump unravelling [55], where the stochastic Schrödinger equation, governing the wavefunction $|\psi(t)\rangle$, has the form

$$d|\psi(t)\rangle = \left\{ dt \left(\hat{1} - i\hat{H}_{\text{eff}} + \frac{1}{2} \sum_i \langle \hat{L}_i^\dagger \hat{L}_i \rangle \right) + \right. \\ \left. + \sum_i dN_i(t) \left(\frac{\hat{L}_i}{\sqrt{\langle \hat{L}_i^\dagger \hat{L}_i \rangle_t}} - \hat{1} \right) \right\} |\psi(t)\rangle , \quad (5)$$

where we define $\langle \hat{L}_i^\dagger \hat{L}_i \rangle_t = \langle \psi(t) | \hat{L}_i^\dagger \hat{L}_i | \psi(t) \rangle$. In Eq. (5), the term $-i\hat{H}_{\text{eff}} |\psi(t)\rangle dt$ gives a deterministic contribution to the evolution of the state with a non-Hermitian Hamiltonian of the form

$$\hat{H}_{\text{eff}} = \hat{H}_{\text{SSH}} - \frac{i}{2} \sum_i \hat{L}_i^\dagger \hat{L}_i , \quad (6)$$

while the c-number term in the first bracket is needed in order to keep the state normalized. The second term on the r.h.s. — the fluctuation term — is the one that makes the differential equation stochastic. Indeed, $dN_i(t) = N_i(t+dt) - N_i(t)$ represents the number of *jumps* of type i the state goes across as a result of a *measurement* made by the environment in the time interval dt . This is a stochastic variable with expectation value

$$E[dN_i(t)] = \langle \hat{L}_i^\dagger \hat{L}_i \rangle_t dt . \quad (7)$$

Since we consider $dt \rightarrow 0$, we can assume $dN_i(t)$ will follow a Poissonian distribution [56], so that

$$dN_i(t) = \begin{cases} 1 & \text{with probability } \langle \hat{L}_i^\dagger \hat{L}_i \rangle_t dt \\ 0 & \text{with probability } 1 - \langle \hat{L}_i^\dagger \hat{L}_i \rangle_t dt \end{cases} . \quad (8)$$

The key advantage of the unravelling method is that it requires evolving a pure state instead of a density matrix, resulting in a substantial reduction in computational complexity. However, this comes with the cost of averaging over many stochastic realizations of the time evolution. Nevertheless, by resorting to parallel computation, this issue becomes manageable, making the method highly efficient [57].

Most importantly, by means of Eq. (5) we will be able to analyze the disconnected entanglement entropy, defined on pure states. The subsequent averaging over trajectories, being the entropy a non-linear function of the state, will provide results that are not attainable by an analysis of the density matrix and its Lindblad evolution. In other words, the trajectory approach allows us to isolate the pure quantum correlations in the state that evolves in time, which is essential for detecting topological phases.

III. DISCONNECTED ENTANGLEMENT ENTROPY ALONG QUANTUM TRAJECTORIES

Let us consider a connected bipartition of a system into two subsets X and \bar{X} . The von Neumann bipartite entanglement entropy of the subsystem in X is defined as [58]

$$S_X = -\text{Tr}_X (\hat{\rho}_X \log_2 \hat{\rho}_X) = -\sum_j \lambda_j \log_2 \lambda_j , \quad (9)$$

where $\hat{\rho}_X = \text{Tr}_{\bar{X}} \hat{\rho}$ is the reduced density matrix of the system in X and $\{\lambda\}$ is the set of its eigenvalues and $\hat{\rho}$ is a pure state.

By choosing the different bipartitions as shown in Fig. 2, the DEE is defined as [59]

$$S^D = S_A + S_B - S_{A \cup B} - S_{A \cap B} . \quad (10)$$

So defined, the DEE is able to detect the presence of edge modes, thus being equal to 2 in the topological phase or to 0 in the trivial phase for the SSH chain. A disconnected partition is necessary for the definition of a marker of topological phases since the entanglement spectrum of single connected partitions is not able to distinguish the topological character of wave functions [31]. A more detailed explanation of the properties of DEE is provided in Appendix A.

For Gaussian states, computing the entanglement entropy for a subset X of a partition is equivalent to computing the spectrum $\{\zeta\}$ of the reduced covariance matrix \mathbf{G} of the same subsystem, whose matrix elements are

$$G_{\alpha, \beta} = \langle \psi(t) | \hat{c}_\beta^\dagger \hat{c}_\alpha | \psi(t) \rangle = \text{Tr}(\hat{\rho}_X \hat{c}_\beta^\dagger \hat{c}_\alpha) , \quad (11)$$

where $\alpha, \beta \in X$ [60] and $|\psi(t)\rangle$ being the state along the considered quantum trajectory.

Since the dissipative dynamics is quadratic, hence preserving the Gaussianity of the initial state, we directly evolve the covariance matrix of the reduced system (11) on each single trajectory, namely $\mathbf{G}(t)|_{\text{traj}}$. Details on the calculations are provided in Appendix D and in Appendix E. Resorting to the free-fermions techniques of Appendix C, we retrieve $S^D(t)|_{\text{traj}}$ for many trajectories.

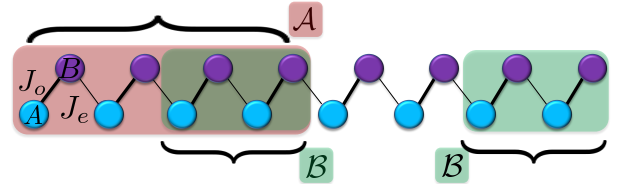


FIG. 2: Disconnected partition of the SSH chain. The red connected subset is named \mathcal{A} , while the green disconnected one is named \mathcal{B} . The blue (odd) sites represent the sublattice indices A , while the purple (even) sites represent the sublattice indices B . J_o and J_e are the intra-cell and inter-cell hopping amplitudes, respectively.

In this sense, the DEE thus becomes a statistical variable. Indeed, by averaging over the trajectories, we can compute its expected value $S^D = \overline{S^D}_{\text{traj}}$ and its counting statistics from a dynamical standpoint.

IV. RESULTS

In this section, we investigate the stability of the topological phase under dissipation by evaluating the DEE along quantum trajectories.

In order to get a first insight on the impact of Lindblad dynamics on the edge states, we first discuss the spreading of the edge modes due to dissipation. Next, we investigate the time-evolution of the expectation value of the DEE under the two types of dissipation — SPD and SBD — outlined in the previous sections.

IV.1. Spreading of the edge modes

The existence of edge states is a well-known characteristics of topological insulators under open boundary conditions. The localization of the edge modes depends on the choice of the ratio J_o/J_e and on the length of the chain [45]. In the limit of perfectly dimerized chain, as shown in Appendix A, the edge modes are exactly localized on the two edge sites. On the contrary, when $J_o/J_e > 0$, the modes have an exponential decay within the bulk of the chain.

As a consequence, owing to the long-range entanglement, the existence of a non-zero correlation among the edge sites of the chain can also characterize a topological state. For instance, the topological order would be disrupted if the boundary modes vanish under the action of a dissipation, and this would be probed by the correlations going to zero as well.

For this reason, we look at the time evolution of the covariance matrix \mathbf{G} , whose matrix elements are

$$G_{ij}(t) = \langle \hat{c}_j^\dagger \hat{c}_i \rangle_t = \text{Tr}(\hat{\rho}(t) \hat{c}_j^\dagger \hat{c}_i), \quad (12)$$

where $i, j \in [1, L]$. Since this is a linear function of the state, we can directly take $\hat{\rho}(t)$ as the solution of the Lindblad equation Eq. (1), without need to use the quantum-trajectory approach. We obtain the equation of motion of the covariance matrix considering that

$$\dot{G}_{ij}(t) = \frac{d}{dt} \text{Tr} \left(\hat{\rho}(t) \hat{c}_j^\dagger \hat{c}_i \right) = \text{Tr} \left(\dot{\hat{\rho}}(t) \hat{c}_j^\dagger \hat{c}_i \right), \quad (13)$$

and inserting Eq. (1) into Eq. (13), so that we get

$$\begin{aligned} \dot{G}_{ij} = & -i (H_{ik} G_{kj} - G_{ik} H_{kj}) + \\ & + \frac{1}{2} \text{Tr} \left\{ \hat{\rho} \hat{L}_k^\dagger \left[\hat{c}_j^\dagger \hat{c}_i, \hat{L}_k \right] + \hat{\rho} \left[\hat{L}_k^\dagger, \hat{c}_j^\dagger \hat{c}_i \right] \hat{L}_k \right\}, \end{aligned} \quad (14)$$

where we sum over repeated indices. In the latter equation, H_{ij} are the matrix elements of \mathbf{H}_{SSH} , which is,

in turn, the matrix representation of the Hamiltonian of Eq. (2) in the fermionic basis, such that $\hat{H}_{\text{SSH}} = \sum_{i,j} \hat{c}_i^\dagger H_{ij} \hat{c}_j$. The solution of the equation of motion, namely $\mathbf{G}(t)$, is an $L \times L$ -dimensional matrix.

When considering the SPD jump operators of Eq. (3), the equation of motion becomes

$$\dot{\mathbf{G}} = -i [\mathbf{H}_{\text{SSH}}, \mathbf{G}] + \gamma (\mathbf{1}_o - \mathbf{G}), \quad (15)$$

where $\mathbf{1}_o$ is a matrix with ones on the odd (A) sites of the diagonal. Considering a site-dependent decay rate, Eq. (15) can be straightforwardly specialized to the case of central α -SPD dissipative dynamics, restricting the $\mathbf{1}_o$ to the cells affected by the dissipation. We notice that the α -SPD dissipation leaves $n = \frac{(1-\alpha)L}{2}$ sites untouched near each edge. Defining ξ as the characteristic localization length of the edge modes (see Appendix 1 for details), we can study the evolution of the correlator $G_{1,L}(t)$ for different values of the ratio $\nu \equiv \frac{n}{\xi} = \frac{(1-\alpha)L}{2\xi}$. In Fig. 3 we show the time evolution of $G_{1,L}$ for different values of α so that the ratio ν becomes progressively larger, once we fix J_o/J_e and the size L of the chain.

Fig. 3(a,b) shows that, the larger is the range of external sites excluded — i.e., the larger is the ratio ν — the slower is the destruction of the correlation. Due to the strong exponential localization of the initial edge mode for $J_o/J_e = 0.1$ ($\xi = 0.43$), in Fig. 3(a) a drastic change in the trend of $G_{1,L}$ appears when passing from $\nu = 5.2$ ($n = 2$, $\alpha = 0.96$) to $\nu = 7.8$ ($n = 3$, $\alpha = 0.94$). By contrast, Fig. 3(b) shows that for less localized edge modes ($\xi = 1.44$), the variation of the trends is more gradual. For α small enough so that $n \gg \xi$, the Lindblad operators act sufficiently far from the range where the initial edge modes are exponentially localized, and in this case the correlator tends to exhibit a constant behavior [see Fig. 3(a,b)]. When this limit is attained, we can talk about a central dissipation, in the sense that it does not involve the edges of the chain [61]. From this preliminary study, we conclude that a fraction of $\alpha = 0.8$ effectively excludes the influence of boundary dissipation.

With this choice for the α -SPD dynamics, we analyze the evolution of the correlator over time for various chain lengths, as shown in Fig. 3(c). Notably, Fig. 3(c) shows that the correlator's saturation occurs in three distinct patterns. This discrete variation arises due to the strong localization of the edge modes. As chain length increases, the number of sites unaffected by dissipation grows as well, resulting in a significant change in dissipation effects due to the steeply decreasing exponential tails of the edge modes along the chain. As a result, the relaxation time in α -SPD increases with L in a discontinuous manner and appears to become infinite for $L \geq 50$, while for global SPD it remains finite and does not vary with L .

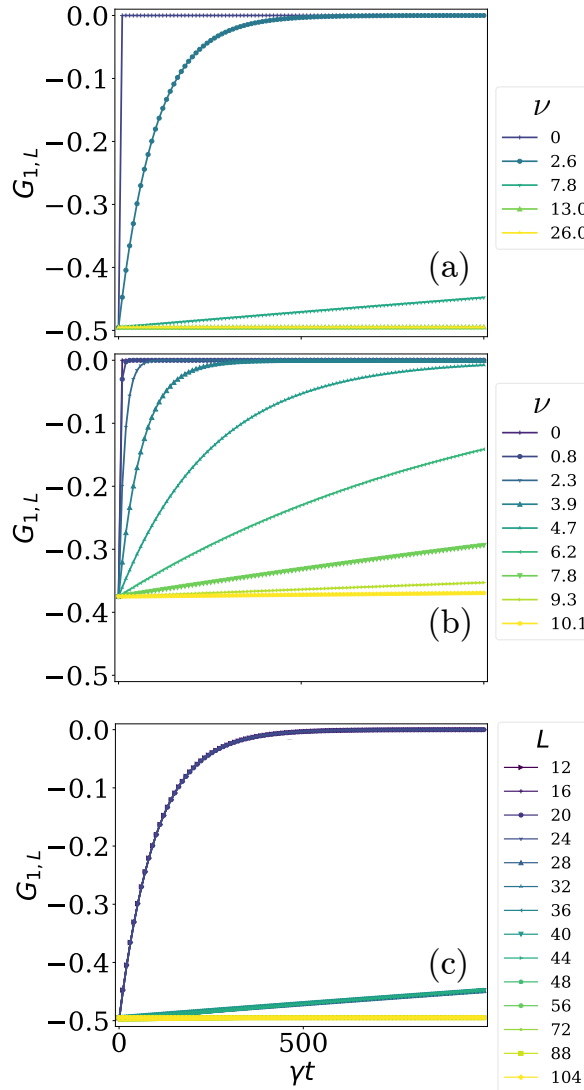


FIG. 3: Two-point correlator for the α -SPD dynamics for $L = 112$ and different values of α decreases. For decreasing α a growing fraction $\nu = \frac{(1-\alpha)L}{2\xi}$ of sites near each edge is left untouched. The system is initialized in the topological half-filled ground state of the Hamiltonian of the isolated SSH chain with parameters $J_o/J_e = 0.1$ — for which $\xi = 0.43$ — in Panel (a) and $J_o/J_e = 0.5$ — for which $\xi = 1.44$ — in Panel (b), with $N = 56$ unit cells ($L = 112$ sites). In Panel (c) α is fixed at 0.8 and L is varied. The system is initialized with $J_o/J_e = 0.1$.

IV.2. Time-evolution of the DEE

In Ref. [32], it has been demonstrated that, in the case of a local, unitary — $\gamma = 0$ — and symmetry-preserving quench, the time at which the DEE deviates from 2 scales linearly with the system size, proving that the DEE is a good non-local order parameter for isolated topological systems in the thermodynamic limit.

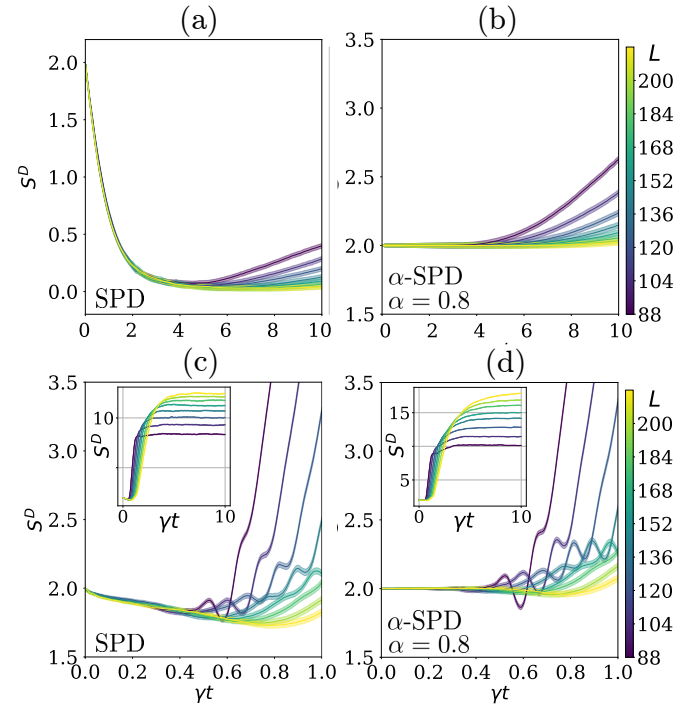


FIG. 4: Dynamics of the DEE under the SPD dynamics with $\gamma = 1$, $J_e/\gamma = 20$ until $\gamma t = 10.0$. (a) Global SPD with topological Hamiltonian ($J_o/J_e = 0.1$), (b) Central α -SPD with $\alpha = 0.8$ and topological Hamiltonian ($J_o/J_e = 0.1$). (c) Global SPD with trivial Hamiltonian ($J_o/J_e = 1.5$) until $\gamma t = 1.0$. (d) Central α -SPD with $\alpha = 0.8$ and trivial Hamiltonian ($J_o/J_e = 1.5$) until $\gamma t = 1.0$. (c,d) Inset plots: whole dynamics until $\gamma t = 10.0$.

Our aim is to extend this study to the dissipative case. To this end, we consider the topological half-filled ground state of \hat{H}_{SSH} with $J_o/J_e = 0.1$ as the initial state of the dynamics. Adopting the techniques described in Appendix C, we calculate the time evolution of the reduced covariance matrix for the subsystems \mathcal{A} , \mathcal{B} , $\mathcal{A} \cup \mathcal{B}$, and $\mathcal{A} \cap \mathcal{B}$ for a single trajectory. From the diagonalisation of the reduced covariance matrix, we calculate the four entanglement entropy contributions that make up the DEE. Once we obtain the estimate of the DEE for a single trajectory, i.e. $S^D|_{\text{traj}}$, we average the result over multiple trajectories ($N_{\text{traj}} = 960$), calculating the error as the standard error.

IV.2.1. DEE in time

In the following, we show the time evolution of the DEE under the global SPD and the central α -SPD dynamics with $\alpha = 0.8$ (see Fig. 4), and global and central SBD dynamics with the same α (see Fig. 5). In each case, we consider different system sizes, from $L = 88$ up to $L = 200$.

In Fig. 4, we show the results for the two SPD dynamics. In Fig. 4(a,b), the Hamiltonian governing the dynamics is topological ($J_o/J_e = 0.1$) and the dissipation is such that $J_e/\gamma = 20$. Fig. 4(a) shows the result for the global SPD dynamics: The initial amount of entanglement is rapidly destroyed due to dissipation. By contrast, Fig. 4(b) shows that the DEE remains quantized to the initial topological value of 2 for central α -SPD dissipation.

We consider also the case of trivial Hamiltonian governing the dynamics ($J_o/J_e = 1.5$) and display the results for the global SPD dissipation in Fig. 4(c) and the central α -SPD one in Fig. 4(d). For this choice of parameters, the two dynamics have a similar qualitative behavior. Yet, the initial plateau of Fig. 4(c) has a non-trivial slope, which is absent in Fig. 4(d). Furthermore, the asymptotic values in Fig. 4(c) are smaller than those of Fig. 4(d). This discrepancy can be only attributed to the presence of quantum jumps on the edge part of the chain in the global SPD dynamics, which are instead absent in the central one. Then, all the curves permanently deviate from the value of 2 at a certain value we refer to as γt_c , and better discuss in Sec. IV.2.2.

In Fig. 5, we show the evolution of the DEE under the SBD dynamics. In Fig. 5(a) the Hamiltonian is topological ($J_o/J_e = 0.1$) and $J_e/\gamma = 20$. As for the global SPD dynamics, the initial topological value of 2 vanishes due to the effect of the global dissipation. In Fig. 5(b) the α -SBD dynamics with the same parameters is shown. The latter shows a greater similarity with the α -SPD case, the DEE remaining constant during the whole dynamics.

In Fig. 5(c) there is a global SBD dissipation with $J_e/\gamma = 20$ and a trivial Hamiltonian ($J_o/J_e = 1.5$). In this case the deviation from the initial value is evident, yet more rapid than in the global SPD case, with an initial shoulder whose scaling behavior is analyzed in the following. Eventually, in Fig. 5(d) the evolution under the α -SBD dynamics under the same parameters is plotted. In it, the presence of the plateau is apparent like in the α -SPD case.

IV.2.2. Scaling with the system size of the deviation time t_c

What we notice in the time traces of Fig. 4 and 5 we notice a deviation of the DEE from the initial topological value of 2 occurring over a certain time scale. We call this time scale deviation time γt_c and estimate it in the following way: For each trajectory, we evaluate $\gamma t_c|_{\text{traj}}$ as the first time at which the threshold condition $|S^D|_{\text{traj}}(t) - S^D|_{\text{traj}}(0)| < (2 \log_2 2)/100$ is met. We estimate $\gamma t_c = \gamma t_c|_{\text{traj}}$ averaging over trajectories. We have checked that different threshold levels provide qualitatively similar results.

The plot in Fig. 6 shows γt_c versus L for the case of central α -SPD dissipation and topological Hamiltonian driving the evolution [see Fig. 4(b)]. We see that t_c linearly

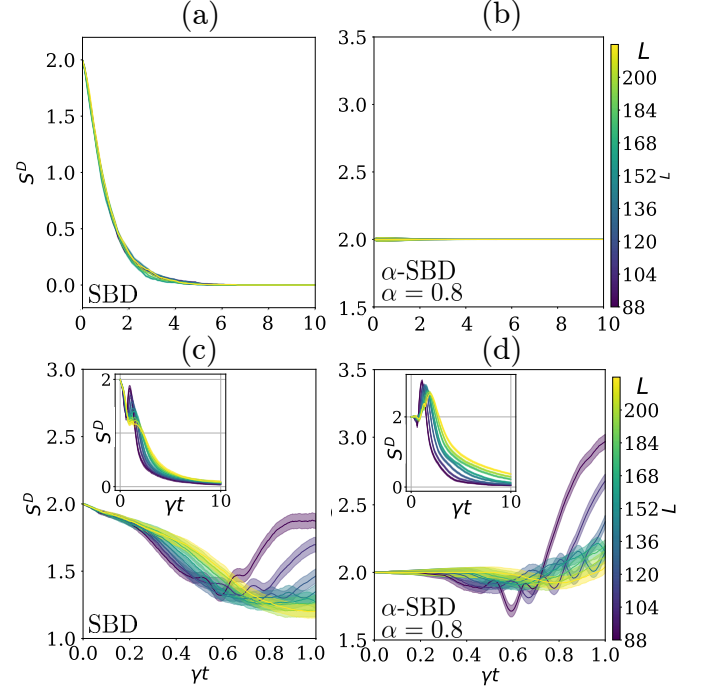


FIG. 5: Dynamics of the DEE under the SBD dynamics with $\gamma = 1$, $J_e/\gamma = 20$ until $\gamma t = 10.0$. (a) Global SPD with topological Hamiltonian ($J_o/J_e = 0.1$), (b) Central α -SBD with $\alpha = 0.8$ and topological Hamiltonian ($J_o/J_e = 0.1$). (c) Global SBD with trivial Hamiltonian ($J_o/J_e = 1.5$) until $\gamma t = 1.0$. (d) Central α -SBD with $\alpha = 0.8$ and trivial Hamiltonian ($J_o/J_e = 1.5$) until $\gamma t = 1.0$. (c,d) Inset plots: whole dynamics until $\gamma t = 10.0$.

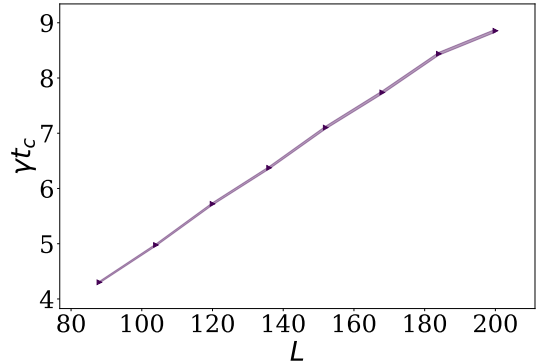


FIG. 6: Linear scaling of γt_c as function of L corresponding to the curves of Fig. 4(b). Topological Hamiltonian ($J_o/J_e = 0.1$), $\gamma = 1$, and $J_e/\gamma = 20$.

increases with L and this shows that when the quantum jumps do not involve the edges of the chain, the DEE remains quantized in the thermodynamic limit.

Fig. 7 shows how γt_c scales with the system size for the three dynamics with the trivial Hamiltonian $J_o/J_e = 1.5$, namely corresponding to the curves of

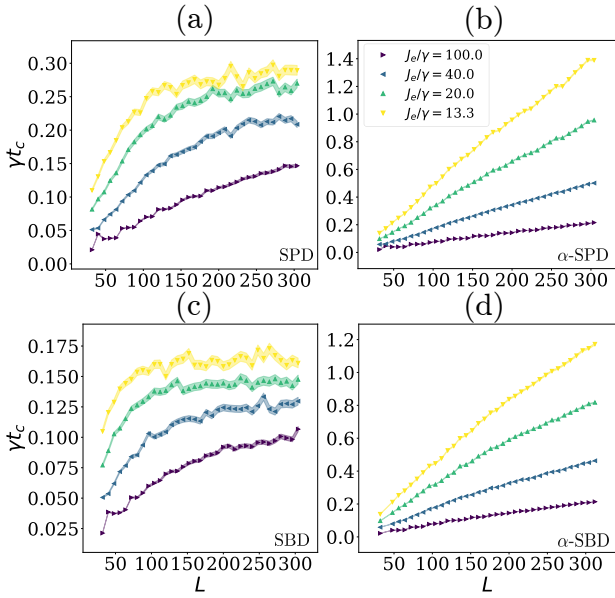


FIG. 7: γt_c versus L with various choices of J_e/γ . (a) Global SPD dynamics. (b) Central α -SPD dynamics with $\alpha = 0.8$. (c) Global SBD dynamics. (d) Central α -SBD dynamics with $\alpha = 0.8$. Trivial Hamiltonian ($J_o/J_e = 1.5$), $\gamma = 1$, and $J_e/\gamma = 20$.

Figs. 4(c), 4(d), 5(c) and 5(d). We see a linear scaling of t_c with L whenever the dissipation is central, both for α -SPD dissipation [see Fig. 6 and 7(b)] and for α -SBD dissipation [see Fig. 7(d)]. Consistently with what occurs in absence of dissipation [32], the linear scaling is not affected by the topological or trivial nature of the Hamiltonian [see Fig. 6 and 7(b).] So, in the case of central dissipation the topological boundary modes are not affected by the Lindbladian, and can remain entangled for a time that diverges in the thermodynamic limit. This effect is the same ofr α -SPD and α -SBD, so it is independent of the symmetry properties of the dissipation

In contrast with that, when the dissipation is global and acts also on the edges of the system, t_c saturates with L . Again this effect is independent of the symmetry properties of the dissipatior and is valid for global SPD [see Fig. 7(b)] and global SBD [see Fig. 7(d)]. Therefore, for global dissipation the entangled topological boundary modes persist only for a finite time, also in the thermodynamic limit.

To summarize, when examining the time evolution of the DEE starting from a topological state, the action of the perturbation on the boundary appears to be the most relevant aspect to consider. In the next section we inquire more deeply this fact by looking at the changes in DEE due to the effect of quantum jumps.

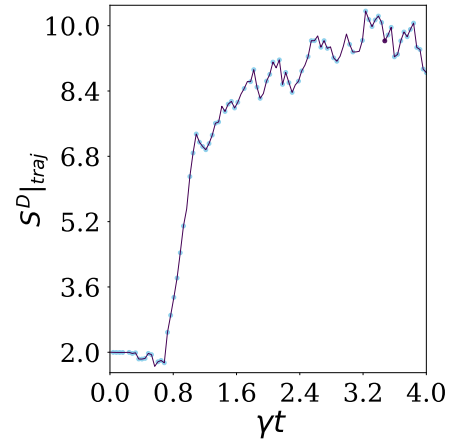


FIG. 8: Time evolution of the DEE over a single trajectory, namely $S^D|_{\text{traj}}$. The blue dots correspond to the occurring of a quantum jump on any site apart from the two edges, where the occurrence of the jump is signalled by a violet dot.

IV.3. Time-resolved statistics of ΔS^D

We can analyze further properties of the DEE dynamics along trajectories. In this section we focus on studying the distribution of the change in DEE due to a quantum jump

We consider the stochastic dynamics of the entanglement entropy along a quantum trajectory. The typical pattern is given by an evolution driven by the non-Hermitian Hamiltonian abruptly interrupted by a discontinuous change in entanglement entropy due to a quantum jump, that we define ΔS^D . Right after the quantum jump, the entanglement entropy can either increase ($\Delta S^D > 0$) or decrease ($\Delta S^D < 0$), as Fig. 8 shows [56, 62]. For this reason, we sample the changes in entanglement entropy at each jump event along a quantum trajectory and repeat this process for different trajectories to generate the histogram $P(\Delta S^D)$.

We show the results of the statistical analysis for the two global-dissipation dynamics in Fig. 9. Specifically, for this and the following section, we consider a chain of $L = 56$ sites and the global SPD dynamics with $J_o/J_e = 0.1$ and $J_e/\gamma = 20$, the global SBD dynamics with same parameters and $\theta = 0$ and the central α -SPD dynamics with $\alpha = 0.8$. The initial state is the topological half-filled ground state of \hat{H}_{SSH} with $J_o/J_e = 0.1$.

The average dynamics generated by Eq. (5) with these parameters allows us to identify two distinct time windows in the evolution of the DEE (cfr. Figs. 4(a) and 5(a)). The first time window goes from $\gamma t_0 = 0.0$ to $\gamma t_f = 4.0$ and coincides with the transient part of the dynamics. The second goes from $\gamma t_0 = 4.0$ to $\gamma t_f = 8.0$ and corresponds to the time interval in which the DEE

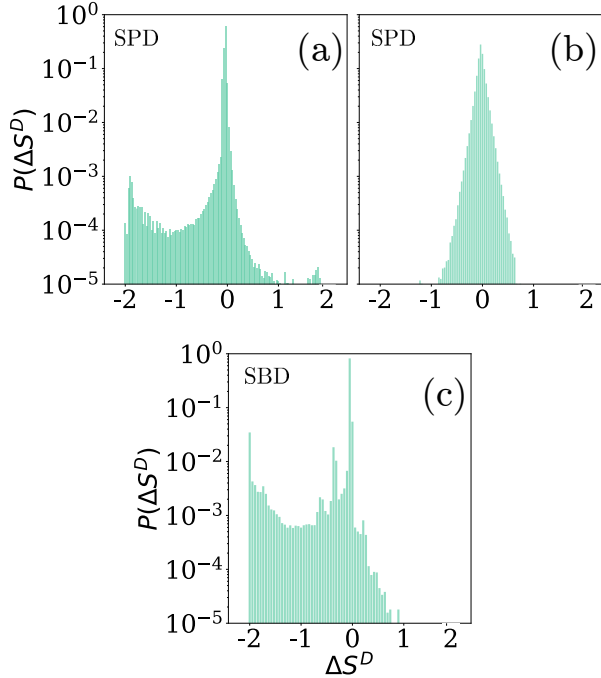


FIG. 9: $P(\Delta S^D)$ for the two different time windows of the two global dynamics. (a) SPD dynamics, $t_0 = 0.0$, $t_f = 4.0$. (b) SPD dynamics, $t_0 = 4.0$, $t_f = 8.0$. (c) SBD dynamics, $t_0 = 0.0$, $t_f = 4.0$. We do not show the statistical analysis related to the second time window for the global SBD dynamics since the chain is emptied by dissipation and no more jumps occur. The initial state is the ground state of \hat{H}_{SSH} with $L = 56$ sites, $J_o/J_e = 0.1$ and the parameters of the dissipative evolution are $\gamma = 1$, $J_o/J_e = 0.1$, $J_e/\gamma = 20$ ($\theta = 0$) and $N_{\text{traj}} = 28800$ trajectories.

approaches its stationary value. We perform a statistical analysis of these windows separately.

In Figs. 9(a,b) we show the results of the statistical analysis for the global SPD case while in Fig. 9(c) we consider the global SBD dynamics. In this latter case, we show only the statistical analysis related to the first time window, because later the chain is emptied by dissipation and no more jumps occur.

The histograms shown in Fig. 9 always exhibit a peak at $\Delta S^D = 0$. However, in the first time window of Fig. 9(a) there is also a second peak at $\Delta S^D = -2$, which makes the distribution bimodal. This peak disappears in the second time window of Fig. 9(b). In Fig. 9(c), apart from the peak at $\Delta S^D = -2$, another at $\Delta S^D \approx -0.38$ is present.

In Fig. 10 we show the same analysis for the central α -SPD and α -SBD dynamics. In Fig. 10(a), the histogram of the central α -SPD dynamics in the first time window is unimodal in contrast with the corresponding case with the global dynamics [see Fig. 9(a)]. The same unimodal

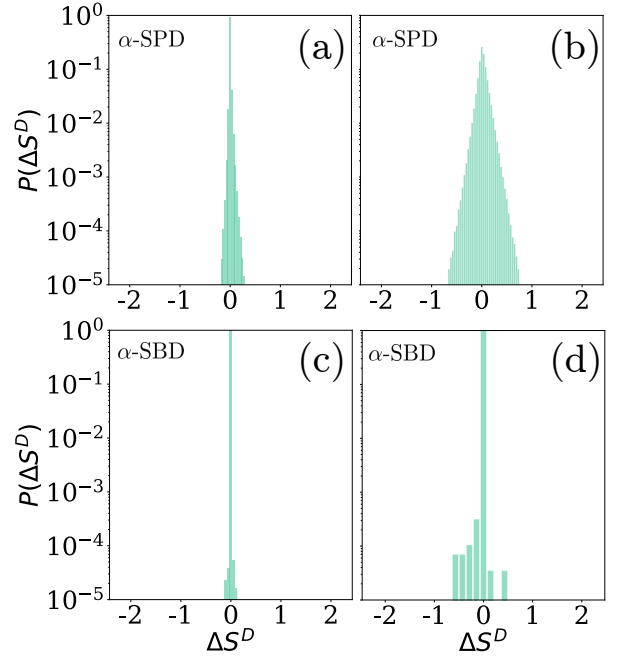


FIG. 10: $P(\Delta S^D)$ for the two different time windows of the central α -SPD dynamics with $\alpha = 0.8$. (a) α -SPD, $t_0 = 0.0$, $t_f = 4.0$. (b) α -SPD, $t_0 = 4.0$, $t_f = 8.0$. (c) α -SBD, $t_0 = 0.0$, $t_f = 4.0$. (d) α -SBD, $t_0 = 4.0$, $t_f = 8.0$.

quality can be observed for α -SPD in the second time window [see Fig. 9(b)] and in the histograms of the central α -SBD dynamics of Figs. 10(c) and 10(d).

So, in summary, we see peaks at values different from $\Delta S^D = 0$ only for a dissipation that acts on the edges, and only for a transient time [the global cases in the first time window shown in Fig. 9(a,c)]. Most remarkably, in this transient, there is a peak occurring at $\Delta S^D = -2$, that is precisely the decrease in DEE occurring if the Bell pair of entangled topological boundary modes is destroyed. This does not occur if the dissipation is central and does not act on the edges.

All that suggests that the global dissipation that acts also on the edges can directly affect the entangled topological boundary modes and destroy them after a finite time, so providing a finite decay time in the thermodynamic limit. In contrast, the central dissipation is not capable of doing it because it does not act on the edges, and has no direct action on the boundary modes. To better confirm this picture, let us consider the site-resolved ΔS^D .

IV.4. Site-resolved statistics of ΔS^D

In this section we conduct a study of the distribution of ΔS^D due to a quantum jump conditioned on the site index where the jump occurs. This analysis is limited to the two global dissipative dynamics. Indeed, the central

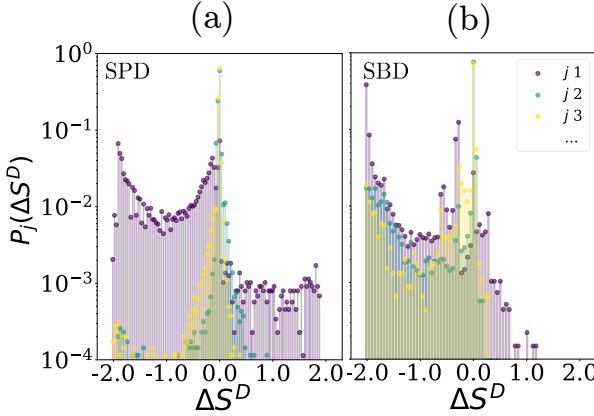


FIG. 11: $P_j(\Delta S^D)$ conditioned on the site where the jump has occurred. (a) Global SPD dynamics. (b) Global SBD dynamics. We focus the statistical analysis in the first time window going from $\gamma t_0 = 0.0$ to $\gamma t_f = 4.0$. The statistical analysis is done considering a sample of $N_{\text{traj}} = 28800$ trajectories.

SPD dynamics would lead to trivial results, since it does not involve the edge sites.

We show the results in Fig. 11. Since the existence of peaks at negative values of ΔS^D has been proven as a characteristic of the first time window of the two global dynamics, we consider only that time window.

For each trajectory, we record the site index j where the jump leading to a ΔS^D occurs, and study separately the histogram of the jumps for each site. For each site j , we call $P_j(\Delta S^D)$ the histogram of the jumps occurring on that site. (It can also be interpreted as conditional probability).

In Fig. 11(a) we consider the SPD dynamics and show $P_j(\Delta S^D)$ versus ΔS^D for different values of j . For each j we take a different color and see that in Fig. 11(a) $P_j(\Delta S^D)$ shows a peak at $\Delta S^D = -2$ only for sites on the edge (that's to say $j = 1$). This confirms the link between the bimodality of the distribution and the destruction of the boundary modes by the action of the dissipator on the edge. Indeed, the destruction of the boundary modes, and their Bell-pair entanglement, gives rise to a $\Delta S^D = -2$, and this occurs only when the jump acts at the boundary and can directly affect the boundary modes, as the peak in $P_j(\Delta S^D)$ for $j = 1$ suggests. In particular, most of the contribution to this peak can be attributed to the first jump that occurs on the boundary sites for each single trajectory, as shown in Appendix F.

In Fig. 11(b) we consider the SBD dynamics and beyond the same peak at $\Delta S^D = -2$ there is also shows a clear peak at $\Delta S^D \simeq -0.38$ when looking at the jumps occurring on the first site. In this case, as proven in Appendix F, owing to the lower locality of the quantum jump, the variation of the DEE after the first jump is not discrete, thus causing the peak at $\Delta S^D = \frac{3}{2} \log_2(3) - 2 \simeq -0.38$. On the contrary, the peak at $\Delta S^D = -2$ is due

to jumps at the boundary occurring at later steps.

Although in different ways, both the statistical analysis of quantum jumps and the study of the dynamics of the DEE confirm the equal destructive effect of the two global dissipation on the entangled pair of boundary modes and on the topological properties of the system. However, they still retain a memory of the initial topological state up to times of order $\sim 1/\gamma$, a fact that is more evident in this latest statistical analysis than in the temporal evolution of the DEE.

V. DISCUSSION AND CONCLUSIONS

In this manuscript, we examined the effects of two dissipative dynamics – Symmetry-Preserving Dissipation (SPD), and Symmetry-Breaking Dissipation (SBD), on the Su-Schrieffer-Heeger model. To better understand the impact of the dissipation on the boundary modes that characterize the topological state in which the model is initialized, we also examined the effects of the dissipation involving only a central portion of the chain.

In this context, we have formulated a framework to characterize topological properties through quantum trajectories. By employing this approach, we observed that the effects of dissipation on topological edge modes are not uniformly distributed throughout the system. Specifically, dissipation acts more significantly on the boundary states compared to the bulk, where its impact remains relatively minimal.

One of the central quantities analyzed in this study is the Disconnected Entanglement Entropy (DEE). We have generalized its definition as the average value of the DEEs computed over multiple trajectories and studied its evolution under the different types of dissipative dynamics. Through our analysis, we demonstrated that under the effect of dissipation, the DEE initially retains its quantized value of 2, reflecting the presence of the topological edge states. However, when dissipation directly affects the boundaries, the DEE deviates from this value, signaling the breakdown of long-range entanglement. In contrast, when dissipation is confined to the bulk, the DEE remains stable, protecting the edge modes. This behavior emphasizes that the location of dissipation is critical in determining the stability of topological phases.

To further understand the role of dissipation on the system's topological properties, we performed a detailed statistical analysis of the quantum jumps. In this analysis, we focused on the discrete changes in the DEE caused by individual quantum jumps, sampling the variations in the DEE throughout different quantum trajectories. We also considered the time-resolved statistics, distinguishing between early and late stages of the system's evolution under dissipation. The results revealed key differences between bulk and boundary dissipation, with quantum jumps on the edge sites contributing more significantly to the disruption of the topological order. Additionally, by studying the site-resolved statistics, we

observed that jumps occurring at the boundary led to changes in the DEE corresponding to an entangled Bell pair, confirming that precisely these jumps were responsible for the destruction of the topological boundary modes.

Finally, our study shows that despite the symmetry differences between SPD and SBD dissipation [6], both lead to similar effects on the edge modes of the topological state in which the system is initialized. Nevertheless, it is important to consider that our analysis offers valuable information about the persistence of the topological properties of the initial state, but does not fully capture the topological characteristics of the dissipation driving the dynamics. Consequently, it is important to acknowledge that our understanding of the topological nature of the dissipation may not be complete. Just as a system evolving under a trivial Hamiltonian can still preserve certain initial topological features [32], the same might hold for trivial dissipation — such as the central α -SBD case we analyzed — which, despite being trivial, preserves the entangled topological modes. A key challenge remains that of identifying a dynamical quantity that can comprehensively capture the impact of trivial or topological dissipation.

Future work should explore this by considering different types of dissipation, different symmetry classifications [7] or different dynamical topological markers to further clarify the role of dissipation in topological phases. Furthermore, it would be interesting to examine the asymptotic value of the DEE, which, in our case, had no relevance from a topological standpoint.

ACKNOWLEDGMENTS

We would like to thank Marcello Dalmonte for very helpful discussions. G. P. acknowledges computational resources from the CINECA award under the ISCRA initiative, and from MUR, PON Ricerca e Innovazione 2014-2020, under Grant No. PIR01_00011 - (I.Bi.S.Co.). This work was supported by PNRR MUR project PE00000023 - NQSTI, by the European Union's Horizon 2020 research and innovation programme under Grant Agreement No 101017733, by the MUR project CN_00000013-ICSC (P.L.), and by the QuantERA II Programme STAQS project that has received funding from the European Union's Horizon 2020 research and innovation programme under Grant Agreement No 101017733 (P.L.). This work is co-funded by the European Union (ERC, RAVE, 101053159) (R.F.). Views and opinions expressed are however those of the authors only and do not necessarily reflect those of the European Union or the European Research Council. Neither the European Union nor the granting authority can be held responsible for them.

Appendix A: Details on the fully dimerized limit of the SSH chain and DEE

1. Edge modes

Considering the Hamiltonian of Eq. (2) with space-dependent couplings [45],

it is straightforward to see that, in the thermodynamic limit, two zero-energy eigenmodes of the Hamiltonian can be found in the form

$$|L\rangle = \sum_{i=1}^N a_i \hat{c}_{i,A}^\dagger |0\rangle = \sum_{i=1}^N a_i |i, A\rangle, \quad (\text{A1a})$$

$$|R\rangle = \sum_{i=1}^N b_i \hat{c}_{i,B}^\dagger |0\rangle = \sum_{i=1}^N b_i |i, B\rangle, \quad (\text{A1b})$$

which are states exponentially localized on either the first site A or the last site B of the chain. In (A1), the coefficients are given by

$$a_i = - \prod_{j=1}^{i-1} \frac{J_{oj}}{J_{ej}} a_1 \quad i = 2, \dots, N \quad (\text{A2a})$$

$$b_i = b_N \frac{-J_{oN}}{J_{ei}} \prod_{j=i+1}^{N-1} \frac{-J_{oj}}{J_{ej}} \quad i = 1, \dots, N-1 \quad (\text{A2b})$$

$$b_1 = a_N = 0. \quad (\text{A2c})$$

The condition Eq. (A2c) is instead incompatible with the existence of zero-energy modes and one must consider the small lift Δ — which is exponentially decaying in the system's size — in the degeneracy between the two edge states. The best approximations of the two edge states are thus the two orthogonal real equal-weighted superpositions of the two. This superposition generates an additional saturated contribution to the entanglement entropy of a partition that includes one edge without the second, like \mathcal{A} and \mathcal{B}/\mathcal{A} in Fig. 2. More precisely, in the fully dimerized topological limit, we can write

$$|L\rangle = \hat{c}_{1,A}^\dagger |0\rangle = |1_{1A} 0_{NB}\rangle \quad (\text{A3a})$$

$$|R\rangle = \hat{c}_{N,B}^\dagger |0\rangle = |0_{1A} 1_{NB}\rangle \quad (\text{A3b})$$

we can write the density matrix of the superposition (singlet) state as

$$\begin{aligned} \hat{\rho}_{AB} = & \frac{1}{2} [|1_{1A} 0_{NB}\rangle \langle 0_{NB} 1_{1A}| + |0_{1A} 1_{NB}\rangle \langle 1_{NB} 0_{1A}| + \\ & + |1_{1A} 0_{NB}\rangle \langle 1_{NB} 0_{1A}| + |0_{1A} 1_{NB}\rangle \langle 0_{NB} 1_{1A}|]. \end{aligned} \quad (\text{A4})$$

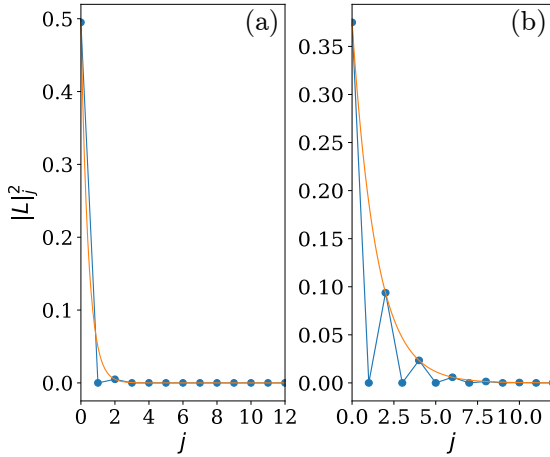


FIG. 12: Edge modes distribution for a topological Hamiltonian with (a) $J_o/J_e = 0.1$ (b) $J_o/J_e = 0.5$. Blue curve: probability amplitude. Orange curve: exponential fit $|L|_j^2 = e^{-j/\xi}$.

When the chain is not in the perfectly dimerized limit, the edge modes (specifically, their probability distribution $|L|_j^2$ or $|R|_j^2$) decay exponentially into the bulk as function of the site index j , as shown in Fig. 12 for the left edge mode, without loss of generality. By fitting an exponential function, we estimate the characteristic localization length ξ of the decay $|L|_j^2 = e^{-j/\xi}$, where j is the site index.

2. Disconnected entanglement entropy

It is thus possible to analytically understand the role of the DEE in the fully-dimerized and topological limit of the SSH chain and show that the ground state always contains the maximally entangled superposition of the two edge states in the topological phase. The reduced system is thus

$$\hat{\rho}_{\mathcal{B}} = \frac{1}{2} [|0_{N\mathcal{B}}\rangle\langle 0_{N\mathcal{B}}| + |1_{N\mathcal{B}}\rangle\langle 1_{N\mathcal{B}}|], \quad (\text{A5})$$

so that $S_{B_{\text{edge}}} = S_{A_{\text{edge}}} = \log_2 2$. This extra contribution is added to the other bulk contributions which depend on the cuts of the chosen partitions.

In the thermodynamic limit it can be easily shown [32] that the latter give a zero contribution, so that only the edge contribution survives and $\lim_{L \rightarrow \infty} S^D = 2 \log_2 2$. More generally, in the thermodynamic limit, the value of S^D is fixed by the number of edge states \mathcal{D} , which is in turn fixed by the bulk-boundary correspondence [63], i.e., $\lim_{L \rightarrow \infty} S^D = \log_2 \mathcal{D}$. For this reason, the DEE is said to correspond to the thermodynamic entropy at zero temperature of one edge [32].

Appendix B: Details on symmetry classifications for open systems

1. Nambu Formalism

Let \hat{c}_j be the destruction operator for a system of spinless fermions labelled by $j = 1, \dots, L$. We define a Nambu column vector $\hat{\mathbf{C}}$ and its Hermitian conjugate row vector $\hat{\mathbf{C}}^\dagger$, each of length $2L$, by [64]

$$\hat{\mathbf{C}} = \begin{pmatrix} \hat{c}_1 \\ \vdots \\ \hat{c}_L \\ \hat{c}_1^\dagger \\ \vdots \\ \hat{c}_L^\dagger \end{pmatrix}, \quad (\text{B1})$$

and

$$\hat{\mathbf{C}}^\dagger = (\hat{c}_1^\dagger, \dots, \hat{c}_L^\dagger, \hat{c}_1, \dots, \hat{c}_L). \quad (\text{B2})$$

Majorana fermions are Hermitian combinations of ordinary complex fermions:

$$\check{\mathbf{c}} = \begin{pmatrix} \check{c}_1 \\ \check{c}_2 \end{pmatrix}, \quad (\text{B3})$$

where \check{c}_1 and \check{c}_2 are L -dimensional (column) vectors whose elements are:

$$\check{c}_{1,j} = (\hat{c}_j^\dagger + \hat{c}_j) \quad \text{and} \quad \check{c}_{2,j} = i(\hat{c}_j^\dagger - \hat{c}_j). \quad (\text{B4})$$

These operators are manifestly Hermitian. They allow us to express the original fermions as:

$$\hat{c}_j = \frac{1}{2}(\check{c}_{1,j} + i\check{c}_{2,j}) \quad \text{and} \quad \hat{c}_j^\dagger = \frac{1}{2}(\check{c}_{1,j} - i\check{c}_{2,j}), \quad (\text{B5})$$

and satisfy the anti-commutation relations:

$$\{\check{c}_{\alpha,j}, \check{c}_{\alpha',j'}\} = 2\delta_{\alpha,\alpha'}\delta_{j,j'}. \quad (\text{B6})$$

To be consistent with the Nambu notation for the ordinary fermions, we better define the Majorana column vector [65]:

$$\check{\mathbf{c}} = \mathbf{W} \hat{\mathbf{C}}, \quad (\text{B7})$$

where we defined the $2L \times 2L$ block matrix:

$$\mathbf{W} = \begin{pmatrix} \mathbf{1} & \mathbf{1} \\ -i\mathbf{1} & i\mathbf{1} \end{pmatrix} \quad \text{such that} \quad \mathbf{W}\mathbf{W}^\dagger = \mathbf{W}^\dagger\mathbf{W} = 2\mathbf{1}. \quad (\text{B8})$$

2. Symmetry classes for open systems: review of the tenfold classification of quadratic Lindbladians

We review the symmetry classification for quadratic open Markovian systems proposed in Ref. [6]. We start

by writing the quadratic Hamiltonian in Eq. (2) and the linear jump operators in terms of the $2L$ Majorana operators $\{\check{c}_j\}$ defined in Eq. (B5) such that

$$\hat{H}_{\text{SSH}} = \sum_{j,j'=1}^{2L} \check{c}_j \mathbf{H}_{j,j'}^{\text{M}} \check{c}_{j'} , \quad (\text{B9a})$$

$$\hat{L}_{\mu} = \sum_{j=1}^{2L} \ell_{\mu j} \check{c}_j , \quad (\text{B9b})$$

where $\mathbf{H}_{j,j'}^{\text{M}}$ are the matrix elements of a $2L \times 2L$ matrix \mathbf{H}^{M} which is purely imaginary and anti-symmetric, $\mathbf{H}^{\text{MT}} = -\mathbf{H}^{\text{M}}$, while $\ell_{\mu j} \in \mathbb{C}$. The superscript in \mathbf{H}^{M} underlines the fact that the Hamiltonian is written in the Majorana operators basis. The dissipation is encoded into a $2L \times 2L$ complex (semi)-positive definite Hermitian matrix \mathbf{M} whose elements are $M_{j,j'} = \sum_{\mu} \ell_{\mu j} \ell_{\mu j'}^*$. Since $\mathbf{M}^* = \mathbf{M}^{\text{T}}$, the real part of \mathbf{M} , $\mathbf{M}_{\text{R}} = \frac{1}{2}(\mathbf{M} + \mathbf{M}^*)$, is a (semi)-positive definite symmetric matrix, while the imaginary part, $\mathbf{M}_{\text{I}} = \frac{1}{2i}(\mathbf{M} - \mathbf{M}^*)$, is anti-symmetric. (One can show that \mathbf{M}_{R} and \mathbf{M}_{I} are associated, respectively, to dissipation and driving [66].)

We now rely on the third-quantization formalism [66, 67] to vectorize the Lindblad equation as

$$\frac{d}{dt} |\hat{\rho}\rangle = \hat{\mathcal{L}} |\hat{\rho}\rangle . \quad (\text{B10})$$

According to this formalism, one expands $|\hat{\rho}\rangle$ into a basis of vectors (Hermitian operators) $\{|P_{\underline{\alpha}}\rangle\}$ of a $2^{2L} = 4^L$ -dimensional space:

$$|P_{\underline{\alpha}}\rangle \stackrel{\text{def}}{=} 2^{-L/2} \check{c}_1^{\alpha_1} \cdots \check{c}_{2L}^{\alpha_{2L}} , \quad \alpha_j = 0, 1 . \quad (\text{B11})$$

We then define [66, 67] the action of fermionic superoperators on this space as follows:

$$\begin{cases} \hat{a}_j |P_{\underline{\alpha}}\rangle = \delta_{\alpha_j,1} |\check{c}_j P_{\underline{\alpha}}\rangle \\ \hat{a}_j^\dagger |P_{\underline{\alpha}}\rangle = \delta_{\alpha_j,0} |\check{c}_j P_{\underline{\alpha}}\rangle . \end{cases} \quad (\text{B12})$$

In terms of these, the Lindbladian can be represented as a quadratic superoperator of the form

$$\hat{\mathcal{L}} = (\hat{\mathbf{a}}^\dagger, \hat{\mathbf{a}}^{\text{T}}) \begin{pmatrix} -\mathbf{X}^{\text{T}} & i\mathbf{Y} \\ \mathbf{0} & \mathbf{X} \end{pmatrix} \begin{pmatrix} \hat{\mathbf{a}} \\ \hat{\mathbf{a}}^{\dagger \text{T}} \end{pmatrix} - \text{Tr} \mathbf{X} \quad (\text{B13})$$

Here, $\hat{\mathbf{a}} = (\hat{a}_1, \dots, \hat{a}_{2L})^{\text{T}}$ is a $2L$ -dimensional column vector formed with the \hat{a}_j operators, $\hat{\mathbf{a}}^\dagger = (\hat{a}_1^\dagger, \dots, \hat{a}_{2L}^\dagger)$ the corresponding row vector, the $2L \times 2L$ real matrix \mathbf{X} is given by

$$\mathbf{X} = -2i\mathbf{H}^{\text{M}} + 2\mathbf{M}_{\text{R}} . \quad (\text{B14})$$

and the $2L \times 2L$ real anti-symmetric matrix $\mathbf{Y} = 4\mathbf{M}_{\text{I}}$. Quite importantly, $\mathbf{X} + \mathbf{X}^{\text{T}} = 4\mathbf{M}_{\text{R}}$ is (semi)-positive definite.

Due to the upper triangular nature of the Lindbladian, its spectral properties are completely determined by the spectrum of \mathbf{X} , i.e., by the set of *rapidities* $\{\beta_j\}$ [66, 67], with $\text{Re}\beta_j \geq 0$. Hence, it is possible to state symmetry relations for \mathbf{X} that generalize the tenfold way classification of topological insulators [68, 69] when in interaction with an environment, as long as the dissipative dynamics can be described by quadratic Lindbladians. Like the Hamiltonian for closed systems, \mathbf{X} becomes now the landmark to check whether the symmetries are preserved or broken and, consequently, if the topological features of the open systems can be preserved or not. Indeed, for closed systems, according to the presence or absence of the following three time-reversal, particle-hole and chiral symmetries (TRS, PHS, Chiral)

$$\begin{aligned} \mathbf{H}^{\text{M}} &= \mathbf{U}_{\text{T}} \mathbf{H}^{\text{M}*} \mathbf{U}_{\text{T}}^\dagger & \mathbf{U}_{\text{T}} \mathbf{U}_{\text{T}}^* &= \pm \mathbf{1} & \text{(TRS)} \\ \mathbf{H}^{\text{M}} &= -\mathbf{U}_{\text{C}} \mathbf{H}^{\text{M}*} \mathbf{U}_{\text{C}}^\dagger & \mathbf{U}_{\text{C}} \mathbf{U}_{\text{C}}^* &= \pm \mathbf{1} & \text{(PHS)} \\ \mathbf{H}^{\text{M}} &= -\mathbf{U}_{\text{S}} \mathbf{H}^{\text{M}} \mathbf{U}_{\text{S}}^\dagger & \mathbf{U}_{\text{S}}^2 &= \mathbf{1} & \text{(Chiral)} \end{aligned} \quad (\text{B15})$$

where $\mathbf{U}_{\text{T,C,S}}$ are all unitary operators, and $\mathbf{U}_{\text{S}} = \mathbf{U}_{\text{C}} \mathbf{U}_{\text{T}}$, the systems fall in one of the ten symmetry classes related to specific types (\mathbb{Z} , \mathbb{Z}_2 , $2\mathbb{Z}$) of topological states, according to the dimension of the system [68]. For open systems, the generalized equations become

$$\begin{aligned} \mathbf{X} &= \mathbf{U}_{\text{T}} \mathbf{X}^{\text{T}} \mathbf{U}_{\text{T}}^\dagger & \mathbf{U}_{\text{T}} \mathbf{U}_{\text{T}}^* &= \pm \mathbf{1} & \text{(TRS)} \\ \mathbf{X} &= \mathbf{U}_{\text{C}} \mathbf{X}^* \mathbf{U}_{\text{C}}^\dagger & \mathbf{U}_{\text{C}} \mathbf{U}_{\text{C}}^* &= \pm \mathbf{1} & \text{(PHS)} \\ \mathbf{X} &= \mathbf{U}_{\text{S}} \mathbf{X}^\dagger \mathbf{U}_{\text{S}}^\dagger & \mathbf{U}_{\text{S}}^2 &= \mathbf{1} & \text{(PAH)} \end{aligned} \quad (\text{B16})$$

where the unitaries have to be the same as those of the closed classification and the Pseudo-Anti-Hermiticity (PAH) symmetry replaces Chiral symmetry. These equations are obtained imposing some physical constraints on the spectrum of the Lindbladian. According to this classification, it is possible to see that the jump operators in Eqs. (3) are symmetry-preserving, while the ones in Eq. (4) are symmetry-breaking.

3. Hamiltonian

Let us start considering the SSH Hamiltonian of Eq. (2). In Nambu formalism it reads as:

$$\hat{H}_{\text{SSH}} = \hat{\mathbf{C}}^\dagger \mathbf{H}_{\text{SSH}} \hat{\mathbf{C}} , \quad (\text{B17})$$

with

$$\mathbf{H}_{\text{SSH}} = \begin{pmatrix} \mathbf{A}_{\text{H}} & \mathbf{0} \\ \mathbf{0} & -\mathbf{A}_{\text{H}} \end{pmatrix} , \quad (\text{B18})$$

where the $L \times L$ real symmetric matrix \mathbf{A}_H reads:

$$\mathbf{A}_H = \frac{1}{2} \begin{pmatrix} 0 & -J_o & 0 & \cdots & \cdots & \cdots & 0 \\ -J_o & 0 & -J_e & 0 & \cdots & \cdots & 0 \\ 0 & -J_e & 0 & -J_o & 0 & \cdots & 0 \\ 0 & 0 & -J_o & 0 & -J_e & \cdots & 0 \\ \vdots & \vdots & \cdots & \ddots & \ddots & \ddots & 0 \\ \vdots & \vdots & \vdots & 0 & -J_e & 0 & -J_o \\ 0 & \cdots & \cdots & \cdots & 0 & -J_o & 0 \end{pmatrix}. \quad (B19)$$

Equivalently, in terms of Majorana operators:

$$\hat{H}_{SSH} = \hat{\mathbf{C}}^\dagger \mathbf{H}_{SSH} \hat{\mathbf{C}} = \check{\mathbf{c}}^T \mathbf{H}_{SSH}^M \check{\mathbf{c}}. \quad (B20)$$

with

$$\mathbf{H}_{SSH}^M = \frac{i}{2} \begin{pmatrix} \mathbf{0} & \mathbf{A}_H \\ -\mathbf{A}_H & \mathbf{0} \end{pmatrix}. \quad (B21)$$

The symmetries that hold for the SSH chain, written in terms of Majorana, are

$$\begin{aligned} \mathbf{H}_{SSH}^M &= -\mathbf{H}_{SSH}^{M*} = \mathbf{U}_T \mathbf{H}_{SSH}^{M*} \mathbf{U}_T^\dagger & (\text{TRS}) \\ \mathbf{H}_{SSH}^M &= \Sigma_z \mathbf{H}_{SSH}^{M*} \Sigma_z = \\ &= -\mathbf{U}_T \Sigma_z \mathbf{H}_{SSH}^{M*} (\mathbf{U}_T \Sigma_z)^\dagger & (\text{PHS}) \\ \mathbf{H}_{SSH}^M &= -\Sigma_z \mathbf{H}_{SSH}^M \Sigma_z^\dagger & (\text{Chiral}) \end{aligned} \quad (B22)$$

where $\mathbf{U}_T = \Sigma_z$ and

$$\Sigma_z = \hat{\sigma}^z \otimes \mathbf{1} \quad (B23)$$

so that $\mathbf{U}_C = \mathbf{U}_T \Sigma_z = \mathbf{1}$ is the operator related to the particle-hole symmetry (PHS) and $\mathbf{U}_S = \Sigma_z$ is the one related to the chiral symmetry (CS). These operators are properly the same we will use to check the symmetries in the dissipative case. The fact that the three symmetries are satisfied, together with the fact that

$$\begin{aligned} \mathbf{U}_T^2 &= \mathbf{U}_T \mathbf{U}_T^* = \mathbf{1} \\ \mathbf{U}_C^2 &= \mathbf{U}_C \mathbf{U}_C^* = \mathbf{1} \\ \mathbf{U}_S^2 &= \mathbf{1} \end{aligned} \quad (B24)$$

makes the system fall into the topological class BDI which provides for a \mathbb{Z} -type of topological invariants, according to the periodic table of topological insulators [69].

4. SPD dynamics

In the SPD dynamics, the dissipation matrix, in terms of Majorana operators, is:

$$\mathbf{M} = \frac{\gamma}{4} \begin{pmatrix} \mathbf{1} & -i(\mathbf{1}_o - \mathbf{1}_e) \\ i(\mathbf{1}_o - \mathbf{1}_e) & \mathbf{1} \end{pmatrix}. \quad (B25)$$

where $\mathbf{1}_o$ is an identity only on the odd (A) sites, and similarly $\mathbf{1}_e$ for the even (B) sites, hence $\mathbf{1} = \mathbf{1}_o + \mathbf{1}_e$.

The real matrix \mathbf{X} appearing in Eq. (B14) is therefore given by:

$$\mathbf{X} \equiv -2i\mathbf{H}_{SSH}^M + 2\mathbf{M}_R = \begin{pmatrix} \frac{\gamma}{2}\mathbf{1} & \mathbf{A}_H \\ -\mathbf{A}_H & \frac{\gamma}{2}\mathbf{1} \end{pmatrix}. \quad (B26)$$

The latter satisfies equations (B16) with the same unitaries of equations (B22).

5. SBD dynamics

In the SBD dynamics the dissipation matrix is:

$$\mathbf{M} = \frac{\gamma}{4} \begin{pmatrix} \mathbf{M}_A & -i\mathbf{M}_A \\ i\mathbf{M}_A & \mathbf{M}_A \end{pmatrix}, \quad (B27)$$

with the complex $L \times L$ matrix \mathbf{M}_A given by:

$$\mathbf{M}_A = \begin{pmatrix} 1 & e^{i\theta} & 0 & \cdots & \cdots & \cdots & 0 \\ e^{-i\theta} & 2 & e^{i\theta} & 0 & \cdots & \cdots & 0 \\ 0 & e^{-i\theta} & 2 & e^{i\theta} & 0 & \cdots & 0 \\ 0 & 0 & e^{-i\theta} & 2 & e^{i\theta} & \cdots & 0 \\ \vdots & \vdots & \cdots & \ddots & \ddots & \ddots & 0 \\ \vdots & \vdots & \vdots & 0 & e^{-i\theta} & 2 & e^{i\theta} \\ 0 & \cdots & \cdots & \cdots & 0 & e^{-i\theta} & 1 \end{pmatrix}. \quad (B28)$$

which does not allow to see the symmetries preserved for \mathbf{X} .

Appendix C: Free-fermions techniques

1. Quadratic Hamiltonians

Let us consider the most general form for a quadratic Hamiltonian

$$\begin{aligned} \hat{\Theta} = \sum_{i,j} & \left[A_{i,j} \hat{c}_i^\dagger \hat{c}_j - A_{i,j}^* \hat{c}_i \hat{c}_j^\dagger + \right. \\ & \left. + B_{i,j} \hat{c}_i \hat{c}_j - B_{i,j}^* \hat{c}_i^\dagger \hat{c}_j^\dagger \right], \end{aligned} \quad (C1)$$

where \mathbf{A} is a Hermitian matrix and \mathbf{B} is a skew-symmetric matrix. This general quadratic Hamiltonian can be also rewritten as [64]

$$\hat{\Theta} = \hat{\mathbf{C}}^\dagger \Theta \hat{\mathbf{C}}, \quad (C2)$$

where

$$\Theta = \begin{pmatrix} \mathbf{A} & \mathbf{B} \\ -\mathbf{B}^* & \mathbf{A}^* \end{pmatrix} \quad (C3)$$

and $\hat{\mathbf{C}}$ is the Nambu operator defined in Eq. (B1).

2. Gaussian states

A Gaussian state is any state whose density matrix can be written as

$$\hat{\rho}(t) = \frac{1}{\mathcal{Z}(t)} e^{-\hat{\Theta}(t)} \quad (\text{C4})$$

where $\mathcal{Z}(t) = \text{Tr } e^{-\hat{\Theta}(t)}$ enforces the normalization. For Gibbs states, $\hat{\Theta}$ is the real quadratic Hamiltonian of the equilibrium state, while, in general, it plays the role of an effective Hamiltonian, which we will refer to as *entanglement Hamiltonian*.

A simpler expression for the Gaussian state can be derived considering a number-preserving $\hat{\Theta}$, i.e.,

$$\hat{H}_{\text{np}} = \sum_{i,j} H_{i,j} \hat{c}_i^\dagger \hat{c}_j. \quad (\text{C5})$$

If $U_{k,\alpha}$ is the i -th component of the k -th eigenstate of \mathbf{H} with eigenvalues ϵ_k , the unitary transformation

$$\hat{c}_i = \sum_k U_{k,i} \hat{a}_k, \quad (\text{C6})$$

allows to diagonalise \hat{H}_{np} and write the Gaussian state as [60, 70]

$$\begin{aligned} \hat{\rho} &= \frac{1}{\mathcal{Z}} e^{-\sum_k \frac{\epsilon_k}{2} (\hat{a}_k^\dagger \hat{a}_k - \hat{a}_k \hat{a}_k^\dagger)} = \\ &= \bigotimes_{k=1}^N \frac{e^{-\frac{\epsilon_k}{2} (\hat{a}_k^\dagger \hat{a}_k - \hat{a}_k \hat{a}_k^\dagger)}}{\mathcal{Z}_k} = \bigotimes_{k=1}^N \frac{\hat{\rho}_k}{\mathcal{Z}_k}, \end{aligned} \quad (\text{C7})$$

where

$$\begin{aligned} \mathcal{Z}_k &= \text{Tr} \left[e^{\frac{\epsilon_k}{2} (\hat{a}_k^\dagger \hat{a}_k - \hat{a}_k \hat{a}_k^\dagger)} \right] = \\ &= 2 \cosh \epsilon_k / 2 = e^{\frac{\epsilon_k}{2}} + e^{-\frac{\epsilon_k}{2}}. \end{aligned} \quad (\text{C8})$$

It is thus trivial to derive the connection between the spectrum of the entanglement Hamiltonian and that of the density matrix.

3. Covariance matrix

As previously done, let us restrict our study to the number-preserving quadratic Hamiltonian of Eq. (C5). Let us consider the covariance matrix of Eq. (11) whose average is computed over the Gaussian state with effective Hamiltonian (C5).

Since $\hat{\rho}$ is a Gaussian state, Wick's theorem holds, and all the higher correlation functions can be expressed in terms of the Hermitian matrix \mathbf{G} . This means that the two-point covariance matrix \mathbf{G} encodes all the necessary information of the Gaussian state [7, 71]. As a limiting case, $\hat{\rho}$ can also be a pure state related to a Slater

determinant, i.e., an eigenstate of an effective Hamiltonian. Diagonalizing $\hat{\Theta}$ with the unitary transformation of Eq. (C6) means having

$$\sum_{i,j} U_{k,i}^* H_{i,j} U_{k',j} = \epsilon_k \delta_{k,k'}. \quad (\text{C9})$$

From the latter equation, we can derive

$$H_{i,j} = \sum_k U_{k,i}^* U_{k,j} \epsilon_k. \quad (\text{C10})$$

Considering Eq. (C10) and the Gaussian state of Eq. (C4), together with the Wick's theorem, we can obtain

$$G_{i,j} = \sum_k U_{k,i}^* U_{k,j} \frac{1}{1 + e^{\epsilon_k}}. \quad (\text{C11})$$

Comparing Eq. (C10) and Eq. (C11), we can deduce that the eigenvalues $\{\epsilon_k\}$ of \mathbf{H} and those $\{\zeta_k\}$ of \mathbf{G} are related by

$$\zeta_k = \frac{1}{1 + e^{\epsilon_k}}, \quad (\text{C12})$$

i.e.,

$$\mathbf{H} = \ln \left[\frac{\mathbf{1} - \mathbf{G}}{\mathbf{G}} \right]. \quad (\text{C13})$$

Eventually, what we have to do is diagonalizing the Hamiltonian. From the unitary diagonalisation matrix \mathbf{U} , we can find the expression of the effective creation and annihilation operators, so that

$$G_{i,j} = \langle \hat{c}_j^\dagger \hat{c}_i \rangle = \sum_{k,k'} \langle \hat{a}_k^\dagger U_{k',j} U_{i,k}^* \hat{a}_k \rangle, \quad (\text{C14})$$

which means that

$$G_{i,j} = \sum_{k=1}^N U_{i,k}^* U_{k,j}, \quad (\text{C15})$$

where N is the number of particles we consider in the system, which, in our half-filling case at zero temperature, coincides with the number of unit cells of the chain.

This approach is faster than direct diagonalisation and allows to compute efficiently, – i.e., by the $N \times N$ matrix \mathbf{G} – the reduced density matrix and its entanglement spectra and S^D .

The representation of the reduced density matrix can be thus written as

$$\begin{aligned} \rho &= \bigotimes_{k=1}^N \frac{1}{\mathcal{Z}_k} \begin{pmatrix} \rho_{k_{11}} & \rho_{k_{10}} \\ \rho_{k_{01}} & \rho_{k_{00}} \end{pmatrix} = \\ &= \bigotimes_{k=1}^N \begin{pmatrix} \frac{e^{-\frac{\epsilon_k}{2}}}{e^{\frac{\epsilon_k}{2}} + e^{-\frac{\epsilon_k}{2}}} & 0 \\ 0 & \frac{e^{\frac{\epsilon_k}{2}}}{e^{\frac{\epsilon_k}{2}} + e^{-\frac{\epsilon_k}{2}}} \end{pmatrix} = \\ &= \bigotimes_{k=1}^N \begin{pmatrix} \zeta_k & 0 \\ 0 & (1 - \zeta_k) \end{pmatrix}, \end{aligned} \quad (\text{C16})$$

which leaves us with the sought connection between the spectra $\{\lambda_k\}$ of ρ and $\{\zeta_k\}$ of \mathbf{G} .

4. Reduced system

When we consider a subsystem of $\{\alpha, \beta\} \in X$ sites, the reduced density matrix $\hat{\rho}_x$ allows to reproduce all expectation values in the subsystem and, as long as it remains Gaussian, so does the *reduced two-point covariance matrix*

$$G_{x\alpha,\beta} = \text{Tr}(\hat{\rho}_x \hat{c}_\beta^\dagger \hat{c}_\alpha). \quad (\text{C17})$$

In order for $\hat{\rho}_x$ to be Gaussian, it is still required to be the exponential of a quadratic effective Hamiltonian, i.e.,

$$\hat{\rho}_x = \mathcal{K} e^{-\hat{H}_x}, \quad (\text{C18})$$

with

$$\hat{H}_x = \sum_{\alpha,\beta} H_{x\alpha,\beta} \hat{c}_\alpha^\dagger \hat{c}_\beta. \quad (\text{C19})$$

Computing the spectrum of the reduced correlation matrix (C17) is equivalent to exactly diagonalizing the entanglement Hamiltonian of the reduced density matrix (C18), yet faster.

Appendix D: Treating the degeneracy of the edge modes

In the preparation of the initial state for the dynamics, we encounter a numerical issue due to the edge mode degeneracy. Specifically, when diagonalizing the Hamiltonian, we find two states with energies close to zero, separated by a gap that decreases exponentially with the system size. Due to this degeneracy, diagonalization routines arbitrarily combine the two eigenstates associated with the nearly degenerate eigenvalue. This leads to problems in constructing the initial correlator, as the zero-energy eigenstates are arbitrarily ordered and combined. As a consequence, the DEE in the initial state is not equal to 2. To overcome this issue, we decide to exploit the parity symmetry of the Hamiltonian.

Indeed, we know that $[\hat{H}_{\text{SSH}}, \hat{P}] = 0$ where \hat{P} is the parity operator whose matrix representation in one dimension acts as

$$\mathbf{P} = \begin{pmatrix} 0 & 0 & \cdots & 0 & 1 \\ 0 & 0 & \cdots & 1 & 0 \\ & \ddots & & & \\ 0 & 1 & \cdots & 0 & 0 \\ 1 & 0 & \cdots & 0 & 0 \end{pmatrix}, \quad (\text{D1})$$

so to invert the first with the last site, the second with the second-last site and so on. Due to this symmetry relation of the SSH Hamiltonian, since both \hat{H}_{SSH} and \hat{P}

are Hermitian, we know it is possible to find a common basis of eigenvectors \mathbf{V}_P such that \mathbf{P} becomes diagonal and \mathbf{H}_{SSH} is reduced into two diagonal blocks of different parity, i.e., $\mathbf{H}_P = \mathbf{V}_P^T \mathbf{H}_{\text{SSH}} \mathbf{V}_P$ such that

$$\mathbf{H}_P = \begin{pmatrix} \mathbf{H}_{\text{odd}} & \\ & \mathbf{H}_{\text{even}} \end{pmatrix}. \quad (\text{D2})$$

Reducing the Hamiltonian into two blocks allows us to split the two degenerate zero modes — one will go in the even block and the other in odd block. Hence, we can diagonalize the two blocks and find the eigenvectors, \mathbf{U}_{odd} and \mathbf{U}_{even} , separately, so to avoid arbitrary numerical superpositions of the two quasi-zero-energy modes. The total matrix of eigenvectors in the rotated basis is

$$\mathbf{U}_P = \begin{pmatrix} \mathbf{U}_{\text{odd}} & \\ & \mathbf{U}_{\text{even}} \end{pmatrix}. \quad (\text{D3})$$

When ordering the eigenvalues in ascending order, we treat the two near-zero-energy modes as degenerate since they differ only beyond the threshold of machine precision ($\sim 10^{-12}$). We place the zero mode of the even block first, followed by the odd-block one. This is because, when constructing the ground state correlator at half-filling, we will sum over all negative energy modes from both the even and odd blocks, up to the sole even zero mode. We choose to populate only the even mode to achieve a spatial configuration of the Bell-like pair between the two edge modes that corresponds to a triplet state $\frac{1}{\sqrt{2}}(|0_1, 1_L\rangle + |1_1, 0_L\rangle)$. Once the eigenvalues and eigenstates are ordered in the rotated basis, we return to the original basis by rotating the eigenstates with \mathbf{V}_P . With these eigenstates, we can finally construct the ground state correlator at half-filling.

Appendix E: Details on the quantum-jump unraveling for quadratic Lindblad equations

1. Quantum-jump unraveling for Gaussian states

We refer to Ref. [72] for more information regarding the adopted algorithm for the computation of the quantum-jump trajectory. Suitably arranging the latter, exploiting the Gaussian nature of the states we deal with, we actually apply the algorithm directly on the covariance matrix related to the Gaussian state, which results in an enormous advantage in terms of computational cost of our calculations. Specifically, we look at the time evolution of $\mathbf{G}(t)|_{\text{traj}}$. In the following we will name $\mathbf{G}(t)|_{\text{traj}}$ as $\mathbf{G}(t)$, for brevity. Nevertheless, it is important to stress that, in the main text, $\mathbf{G}(t)$ is the average over many realizations of $\mathbf{G}(t)|_{\text{traj}}$.

a. Non-Hermitian evolution

Let us now consider the non-Hermitian contribution to the evolution ruled by \hat{H}_{eff} . An efficient way of updat-

ing the state when the non-Hermitian evolution occurs is

considering

$$\mathbf{G}(t + dt) = \langle \psi(t) | \left(\hat{\mathbb{1}} + i\hat{H}_{\text{eff}}^\dagger dt + \Lambda(t)dt \right) \hat{c}_j^\dagger \hat{c}_i \left(\hat{\mathbb{1}} - i\hat{H}_{\text{eff}} dt + \Lambda(t)dt \right) | \psi(t) \rangle + o(dt) \quad (\text{E1})$$

is the part of equation (5) ruling the non-Hermitian evolution of the correlation function including the normalization of the state, valid in $o(dt)$ limit, where we have written

$$\hat{\Lambda} = \frac{\gamma}{2} \sum_k \hat{L}_k^\dagger \hat{L}_k \quad (\text{E2a})$$

$$\Lambda = \langle \psi(t) | \hat{\Lambda} | \psi(t) \rangle \quad (\text{E2b})$$

$$\hat{H}_{\text{eff}} = \hat{H}_{\text{SSH}} - i\hat{\Lambda}. \quad (\text{E2c})$$

This leads to

$$G_{ij}(t + dt) = G_{ij}(t) + idt \langle \psi(t) | [\hat{H}_{\text{SSH}}, \hat{c}_j^\dagger \hat{c}_i] | \psi(t) \rangle - dt \langle \psi(t) | \left\{ \hat{\Lambda}, \hat{c}_j^\dagger \hat{c}_i \right\} | \psi(t) \rangle + 2dt\Lambda G_{ij}(t) + o(dt). \quad (\text{E3})$$

What makes symmetry-breaking and symmetry-preserving case different is $\hat{\Lambda}$, so we will write them in the following. For the unitary part, which is common to both dynamics, we have

$$\langle [\hat{H}_{\text{SSH}}, \hat{c}_j^\dagger \hat{c}_i] \rangle = \sum_\alpha (G_{i,\alpha} H_{\alpha,j} - H_{i,\alpha} G_{\alpha,j}) \quad (\text{E4})$$

2. Evolution of the norm

In order to consider the occurrence of the quantum jump when $\langle \psi(t^*) | \psi(t^*) \rangle > r$, where r is the random number uniformly distributed in $[0, 1]$, we simultaneously compute the time-evolution of the norm $n(t) = \langle \psi(t) | \psi(t) \rangle$ when it evolves under \hat{H}_{eff}

$$n(t + dt) = n(dt) - 2dt n(t) \Lambda(t) + o(dt), \quad (\text{E5})$$

so that

$$\frac{n(t + dt) - n(t)}{dt} = -2\Lambda(t)n(t), \quad (\text{E6})$$

which in $dt \rightarrow 0$ limit is

$$\frac{dn(t)}{dt} = -2\Lambda(t)n(t), \quad (\text{E7})$$

where, again, Λ must be computed in the two dissipative cases.

a. SPD

a.1. Non-Hermitian evolution. In the SPD case we have

$$\hat{\Lambda} = \frac{\gamma}{2} \left[\sum_{\alpha=1}^L (-1)^\alpha \hat{c}_\alpha^\dagger \hat{c}_\alpha \right] + L \frac{\gamma}{4} \quad (\text{E8})$$

which leads to a non-Hermitian evolution of \mathbf{G} of the form

$$\frac{d\mathbf{G}}{dt} = i(\mathbf{GH} - \mathbf{HG}) - \gamma \left[\frac{\mathbf{GS} + \mathbf{SG}}{2} - \mathbf{GSG} \right], \quad (\text{E9})$$

where $\mathbf{S} = \mathbf{1}_o - \mathbf{1}_e$.

a.2. Quantum Jump. In the symmetry-preserving case we have jump operators of the form (3). We discretize the time at intervals dt . At each time step, we call $|\psi_t\rangle$ the state before the time step is performed, define $\hat{c}_{2j-1} = \hat{c}_{j,A}$, $\hat{c}_{2j} = \hat{c}_{j,B}$ and the time-dependent covariance matrix and anomalous covariance matrix, respectively as

$$G_{ij}(t) \equiv \langle \psi_t | \hat{c}_j^\dagger \hat{c}_i | \psi_t \rangle, \quad F_{ij}(t) \equiv \langle \psi_t | \hat{c}_j \hat{c}_i | \psi_t \rangle. \quad (\text{E10})$$

In order to perform the time step, we act on $|\psi_t\rangle$. There are some mutually exclusive possibilities

- For one $l = 1, \dots, N$, with probability

$$dp_l = \gamma dt \langle \psi_t | \hat{c}_{l,A}^\dagger \hat{c}_{l,A} | \psi_t \rangle = \gamma dt G_{2l-1, 2l-1}(t),$$

we apply the transformation

$$|\psi_t\rangle \longrightarrow |\psi_{t+dt}\rangle = \frac{\hat{c}_{2l-1} | \psi_t \rangle}{\| \hat{c}_{2l-1} | \psi_t \rangle \|}. \quad (\text{E11})$$

Assuming that the state remains Gaussian and that

the Wick's theorem holds, this equation translates into an evolution equation for the covariance matrix

$$G_{ij}(t + dt) = \langle \psi_{t+dt} | \hat{c}_j^\dagger \hat{c}_i | \psi_{t+dt} \rangle = \frac{\langle \psi_t | \hat{c}_{2l-1}^\dagger \hat{c}_j^\dagger \hat{c}_i \hat{c}_{2l-1} | \psi_t \rangle}{G_{2l-1, 2l-1}(t)} = G_{ij}(t) + \frac{F_{2l-1, j}^*(t) F_{2l-1, i}(t) - G_{i, 2l-1}(t) G_{2l-1, j}(t)}{G_{2l-1, 2l-1}(t)} \quad (\text{E12})$$

$$F_{ij}(t + dt) = \langle \psi_{t+dt} | \hat{c}_j \hat{c}_i | \psi_{t+dt} \rangle = \frac{\langle \psi_t | \hat{c}_{2l-1}^\dagger \hat{c}_j \hat{c}_i \hat{c}_{2l-1} | \psi_t \rangle}{G_{2l-1, 2l-1}(t)} = F_{ij}(t) + \frac{G_{j, 2l-1}(t) F_{2l-1, i}(t) - G_{i, 2l-1}(t) F_{2l-1, j}(t)}{G_{2l-1, 2l-1}(t)}. \quad (\text{E13})$$

- For one $l = 1, \dots, N$, with probability

$$dq_l = \gamma dt \langle \psi_t | \hat{c}_{lB} \hat{c}_{lB}^\dagger | \psi_t \rangle = \gamma dt [1 - G_{2l, 2l}(t)],$$

we apply the transformation

$$|\psi_t\rangle \longrightarrow |\psi_{t+dt}\rangle = \frac{\hat{c}_{2l}^\dagger |\psi_t\rangle}{\|\hat{c}_{2l}^\dagger |\psi_t\rangle\|}.$$

This reflects into a transformation for the correlation functions

$$G_{ij}(t + dt) = \langle \psi_{t+dt} | \hat{c}_j^\dagger \hat{c}_i | \psi_{t+dt} \rangle = \frac{\langle \psi_t | \hat{c}_{2l} \hat{c}_j^\dagger \hat{c}_i \hat{c}_{2l}^\dagger | \psi_t \rangle}{1 - G_{2l, 2l}(t)} = G_{ij}(t) + \frac{[\delta_{2l, j} - G_{2l, j}(t)][\delta_{i, 2l} - G_{i, 2l}(t)] - F_{i, 2l}(t) F_{j, 2l}^*(t)}{1 - G_{2l, 2l}(t)} \quad (\text{E14})$$

$$F_{ij}(t + \Delta t) = \langle \psi_{t+\Delta t} | \hat{c}_j \hat{c}_i | \psi_{t+\Delta t} \rangle = \frac{\langle \psi_t | \hat{c}_{2l} \hat{c}_j \hat{c}_i \hat{c}_{2l}^\dagger | \psi_t \rangle}{1 - G_{2l, 2l}(t)} = F_{ij}(t) + \frac{F_{j, 2l}(t)[\delta_{j, 2l} - G_{j, 2l}(t)] - F_{i, 2l}[\delta_{j, 2l} - G_{j, 2l}(t)]}{1 - G_{2l, 2l}(t)}. \quad (\text{E15})$$

b. SBD

b.1. Non-Hermitian evolution. In the symmetry-breaking case we have

$$\hat{\Lambda} = \frac{\gamma}{2} \left[\sum_{\alpha=0}^{L-2} \hat{c}_\alpha^\dagger \hat{c}_\alpha + \hat{c}_{\alpha+1}^\dagger \hat{c}_{\alpha+1} + e^{-i\theta} \hat{c}_{\alpha+1}^\dagger \hat{c}_\alpha + e^{i\theta} \hat{c}_\alpha^\dagger \hat{c}_{\alpha+1} \right]. \quad (\text{E16})$$

From which it is straightforward to derive the non-Hermitian evolution of \mathbf{G} as done in the SPD dynamics.

b.2. Quantum Jump. In the symmetry-breaking case we have the jump operators of the form (4). In this case, we can write $\hat{c}_{2j-1} = \hat{c}_{jA}$, $\hat{c}_{2j} = \hat{c}_{jB}$. The mutually exclusive possibilities are

- For one $l = 1, \dots, N$ with probability

$$dp_l = \gamma dt \langle \psi_t | \hat{L}_{2l-1}^\dagger \hat{L}_{2l-1} | \psi_t \rangle = \gamma dt [G_{2l-1, 2l-1} + G_{2l, 2l} + e^{i\theta} G_{2l, 2l-1} + e^{-i\theta} G_{2l-1, 2l}] = \gamma dt N \quad (\text{E17})$$

we apply the transformation

$$|\psi_t\rangle \rightarrow |\psi_{t+dt}\rangle = \frac{\hat{L}_{2l-1} |\psi_t\rangle}{\|\hat{L}_{2l-1} |\psi_t\rangle\|} = \frac{(\hat{c}_{2l-1} + e^{i\theta} \hat{c}_{2l}) |\psi_t\rangle}{\|\hat{c}_{2l-1} + e^{i\theta} \hat{c}_{2l} |\psi_t\rangle\|}$$

So that the correlation matrix, neglecting the

anomalous correlations, becomes

$$G_{i,j}(t + dt) = G_{ij} - \frac{1}{N} \{ G_{i,2l-1} G_{2l-1,j} + G_{i,2l} G_{2l,j} + e^{-i\theta} G_{i,2l} G_{2l-1,j} + e^{i\theta} G_{i,2l-1} G_{2l,j} \} \quad (\text{E18})$$

- For one $l = 1, \dots, N$ with probability

$$d\mathbf{q}_l = \gamma dt [G_{2l,2l} + G_{2l+1,2l+1} + e^{i\theta} G_{2l+1,2l} + e^{-i\theta} G_{2l+1,2l}] = \gamma dt N \quad (\text{E19})$$

we apply the transformation

$$|\psi_t\rangle \rightarrow |\psi_{t+dt}\rangle = \frac{\hat{L}_{2l} |\psi_t\rangle}{\|\hat{L}_{2l} |\psi_t\rangle\|} = \frac{(\hat{c}_{2l} + e^{i\theta} \hat{c}_{2l+1}) |\psi_t\rangle}{\|\hat{c}_{2l} + e^{i\theta} \hat{c}_{2l+1} |\psi_t\rangle\|}$$

$$G_{i,j}(t + dt) = G_{ij} - \frac{1}{N} \{ G_{i,2l} G_{2l,j} + G_{i,2l+1} G_{2l+1,j} + e^{-i\theta} G_{i,2l+1} G_{2l,j} + e^{i\theta} G_{i,2l} G_{2l+1,j} \}. \quad (\text{E20})$$

Appendix F: Effect of the first jump on a 4-sites chain

In the following, we report the effect of the first jump on the ground state of the Hamiltonian in the perfectly-dimerized topological state for a simple example of 4-sites chain. Although extremely simplistic, this example helps understanding the origin of some of the peaks highlighted in the histograms of the index-resolved statistical analysis, in particular the peak at $\Delta S^D = -2$ for the global SPD dynamics and that at $\Delta S^D \simeq -0.38$ for the global SBD dynamics. The simplification of considering the jump as occurring as soon as the initial state is prepared is justified by the observation that the non-Hermitian evolution statistically does not drastically change the amount of entanglement of the initial state.

Let us consider a chain of two unit cells and four sites. We naturally choose a bipartition of the system such that the first two sites belong to \mathcal{A} and the last two belong to \mathcal{B} . Let us consider the local jump operator that acts on the first site of the chain so to give the non-normalized state

$$\begin{aligned} |\psi_{\text{jump}}^{\text{SPD}}\rangle &= \hat{c}_1 |\text{GS}\rangle = \hat{c}_1 \frac{1}{2} (\hat{c}_1^\dagger + \hat{c}_4^\dagger) (\hat{c}_2^\dagger + \hat{c}_3^\dagger) |0\rangle = \\ &= \frac{1}{2} (\hat{c}_2^\dagger + \hat{c}_3^\dagger) |0\rangle, \end{aligned} \quad (\text{F1})$$

which we will write in the following as

$$|\psi_{\text{jump}}^{\text{SPD}}\rangle = \frac{1}{2} (|1_2\rangle + |1_3\rangle). \quad (\text{F2})$$

So that the correlation matrix, still neglecting the anomalous correlations, becomes

In this notation, each state has implicit zero-occupation values on the non-written sites, e.g., $|1_2\rangle$ is implicitly equivalent to $|0_1 1_2 0_3 0_4\rangle$. The corresponding and suitably normalized density matrix will be

$$\begin{aligned} \hat{\rho}^{\text{SPD}} &= |\psi_{\text{jump}}^{\text{SPD}}\rangle \langle \psi_{\text{jump}}^{\text{SPD}}| = \\ &= \frac{1}{2} (|1_2\rangle \langle 1_2| + |1_2\rangle \langle 1_3| + |1_3\rangle \langle 1_2| + |1_3\rangle \langle 1_3|). \end{aligned} \quad (\text{F3})$$

We can then compute the reduced density matrix, so to know the effect of the jump on one of the terms that make up the DEE. In doing the partial trace of this fermionic system we do not encounter ambiguities, since the states we deal with are always superposition of kets of a number of fermions of same (odd) parity [73, 74]. Hence, we trace out the degrees of freedom of sites 3 and 4 and obtain

$$\hat{\rho}_{\mathcal{A}}^{\text{SPD}} = \frac{1}{2} (|0_1 1_2\rangle \langle 0_1 1_2| + |0_1 0_2\rangle \langle 0_1 0_2|), \quad (\text{F4})$$

and its eigenvalues are $\{1/2, 1/2, 0, 0\}$ so that $S_{\mathcal{A}} = 1$ and $\Delta S_{\mathcal{A}} = -1$. Tracing out the degrees of freedom of sites 1,2 and 3 we can also compute the variation of $S_{\mathcal{A} \cup \mathcal{B}}$ since

$$\hat{\rho}_{\mathcal{A} \cup \mathcal{B}}^{\text{SPD}} = \frac{1}{2} (|0_3\rangle \langle 0_3| + |1_3\rangle \langle 1_3|) \quad (\text{F5})$$

so that $S_{\mathcal{A} \cup \mathcal{B}} = 1$ and $\Delta S_{\mathcal{A} \cup \mathcal{B}} = 0$. We can straightforwardly show that $\Delta S_{\mathcal{B}} = -1$ and $\Delta S_{\mathcal{A} \cap \mathcal{B}} = 0$ so to understand why the peak at $\Delta S^D = -2$ in Figs. 9(a) and 11(a) is due to the jump localized on one of the two edge sites.

On the other hand, if the SBD jump operator acts on the first site, without loss of generality, it simultaneously affects the second site, so that the effect of the first jump on the boundary is completely different. In this case, after the jump, we have the non-normalized state

$$|\psi_{\text{jump}}^{\text{SBD}}\rangle = \frac{1}{2} (\hat{c}_1 + \hat{c}_2) (\hat{c}_1^\dagger + \hat{c}_4^\dagger) (\hat{c}_2^\dagger + \hat{c}_3^\dagger) |0\rangle = \\ = \frac{1}{2} \left[(\hat{c}_2^\dagger + \hat{c}_3^\dagger) - (\hat{c}_1^\dagger + \hat{c}_4^\dagger) \right] |0\rangle. \quad (\text{F6})$$

In this case, there is still a trace of the long-range-entangled Bell-like state $\frac{1}{\sqrt{2}} (\hat{c}_1^\dagger + \hat{c}_4^\dagger)$, which causes a totally different and non-discrete variation in the entanglement contributions of the DEE. The corresponding normalized density matrix is

$$\hat{\rho}_{\text{jump}}^{\text{SBD}} = \frac{1}{4} [|1_2\rangle\langle 1_2| + |1_2\rangle\langle 1_3| - |1_2\rangle\langle 1_1| + \\ - |1_2\rangle\langle 1_4| + |1_3\rangle\langle 1_2| + |1_3\rangle\langle 1_3| - |1_3\rangle\langle 1_1| + \\ - |1_3\rangle\langle 1_4| - |1_1\rangle\langle 1_2| - |1_1\rangle\langle 1_3| + |1_1\rangle\langle 1_1| + \\ + |1_1\rangle\langle 1_4| - |1_4\rangle\langle 1_2| - |1_4\rangle\langle 1_3| + |1_4\rangle\langle 1_1| + \\ + |1_4\rangle\langle 1_4|]. \quad (\text{F7})$$

By tracing out the degrees of freedom of sites 3 and 4, we get

$$\hat{\rho}_{\mathcal{A}}^{\text{SBD}} = \frac{1}{4} [|0_{102}\rangle\langle 0_{102}| + |0_{112}\rangle\langle 0_{112}| + \\ - |0_{112}\rangle\langle 1_{102}| - |1_{102}\rangle\langle 0_{112}| + |1_{102}\rangle\langle 1_{102}|], \quad (\text{F8})$$

whose eigenvalues are $\{1/2, 1/2, 0, 0\}$ so that $S_{\mathcal{A}} = 1$ and

$\Delta S_{\mathcal{A}} = -1$. This result is interesting since, after the occurrence of the jump on the boundary, one would expect $S_{\mathcal{A}}$ to go to 0 owing to the action on both the sites 1 and 2 that are part of two distinct Bell-like pairs. On the contrary, the peculiar form of $|\psi_{\text{jump}}^{\text{SBD}}\rangle$ mixes the things in an unexpectable way. Furthermore, we can trace out the degrees of freedom of sites 1, 2 and 3 and see that

$$\hat{\rho}_{\mathcal{A} \cup \mathcal{B}}^{\text{SBD}} = \frac{1}{4} [3|0_3\rangle\langle 0_3| + |1_3\rangle\langle 1_3|] \quad (\text{F9})$$

so that $S_{\mathcal{A} \cup \mathcal{B}} = -\frac{3}{4} \log_2(3) + 2 \simeq 0.81$ and $\Delta S_{\mathcal{A} \cup \mathcal{B}} = -\frac{3}{4} \log_2(3) + 1 \simeq -0.19$. Again, counter-intuitively, the variation is not quantized, and we have numerically verified that, in the limit of perfectly-dimerized chain, this is not a size-dependent result. Again, it is straightforward to show that $\Delta S_{\mathcal{B}} \simeq -1$ and $\Delta S_{\mathcal{A} \cap \mathcal{B}} = -\frac{3}{4} \log_2(3) + 1 \simeq -0.19$ so that $\Delta S^D = 2(-\frac{3}{4} \log_2(3) + 2) \simeq 1.62$. This result is mainly useful to understand that the variation of the DEE in the SBD dynamics is not discrete when the first jump occurs. At the same time, analyzing a single trajectory at larger sizes shows that the variation, although still not discrete, is different and such that $\Delta S^D = 2 - 2(-\frac{3}{4} \log_2(3) + 2) \simeq -0.38$ because $\Delta S_{\mathcal{A}} = -\frac{3}{4} \log_2(3) + 1 \simeq -0.19$, $\Delta S_{\mathcal{B}} = -\frac{3}{4} \log_2(3) + 1 \simeq -0.19$, $\Delta S_{\mathcal{A} \cup \mathcal{B}} \simeq 0$ and $\Delta S_{\mathcal{A} \cap \mathcal{B}} \simeq 0$. This considerations help us in the interpretation of the peak at $\Delta S^D = 2 - 2(-\frac{3}{4} \log_2(3) + 2) \simeq -0.38$ in Figs. 9(c) and 11(b). At the same time, we have numerically verified that the peak at $\Delta S^D = -2$ for the SBD dynamics is due to jumps occurring at the boundary after several other jumps, and thus are not directly involved in the initial destruction of the long-range entangled Bell-like state.

[1] S. Basu, *Topological Phases in Condensed Matter Physics* (Springer Nature Singapore, 2023).

[2] Y. Ashida, Z. Gong, and M. Ueda, *Advances in Physics* **69**, 249–435 (2020).

[3] N. Okuma and M. Sato, *Annual Review of Condensed Matter Physics* **14**, 83–107 (2023).

[4] S. Diehl, E. Rico, M. A. Baranov, and P. Zoller, *Nature Physics* **7**, 971–977 (2011).

[5] C.-E. Bardyn, M. A. Baranov, C. V. Kraus, E. Rico, A. İmamoğlu, P. Zoller, and S. Diehl, *New Journal of Physics* **15**, 085001 (2013).

[6] S. Lieu, M. McGinley, and N. R. Cooper, *Physical Review Letters* **124**, 10.1103/physrevlett.124.040401 (2020).

[7] A. Altland, M. Fleischhauer, and S. Diehl, *Physical Review X* **11**, 10.1103/physrevx.11.021037 (2021).

[8] A. Altland and M. R. Zirnbauer, *Physical Review B* **55**, 1142 (1997).

[9] K. Kawabata, K. Shiozaki, M. Ueda, and M. Sato, *Phys. Rev. X* **9**, 041015 (2019).

[10] D. Bernard and A. LeClair, A classification of non-hermitian random matrices, in *Statistical Field Theories* (Springer Netherlands, 2002) p. 207–214.

[11] T. Prosen, *Phys. Rev. Lett.* **109**, 090404 (2012).

[12] B. Buca and T. Prosen, *New Journal of Physics* **14**, 073007 (2012).

[13] V. V. Albert and L. Jiang, *Phys. Rev. A* **89**, 022118 (2014).

[14] J. Huber, P. Kirton, S. Rotter, and P. Rabl, *SciPost Phys.* **9**, 052 (2020).

[15] M. Kawasaki, K. Mochizuki, and H. Obuse, *Physical Review B* **106**, 10.1103/physrevb.106.035408 (2022).

[16] F. K. Kunst, E. Edvardsson, J. C. Budich, and E. J. Bergholtz, *Physical Review Letters* **121**, 10.1103/physrevlett.121.026808 (2018).

[17] Z. Gong, Y. Ashida, K. Kawabata, K. Takasan, S. Higashikawa, and M. Ueda, *Physical Review X* **8**, 10.1103/physrevx.8.031079 (2018).

[18] H. Shen, B. Zhen, and L. Fu, *Phys. Rev. Lett.* **120**, 146402 (2018).

[19] O. Viyuela, A. Rivas, and M. A. Martin-Delgado, *Phys. Rev. Lett.* **112**, 130401 (2014).

[20] O. Viyuela, A. Rivas, S. Gasparinetti, A. Wallraff, S. Filipp, and M. A. Martin-Delgado, *npj Quantum Information* **4**, 10.1038/s41534-017-0056-9 (2018).

[21] A. Carollo, B. Spagnolo, and D. Valenti, *Uhlmann curvature in dissipative phase transitions* (2017),

arXiv:1710.07560 [quant-ph].

[22] C.-E. Bardyn, L. Wawer, A. Altland, M. Fleischhauer, and S. Diehl, *Phys. Rev. X* **8**, 011035 (2018).

[23] R. Unanyan, M. Kiefer-Emmanouilidis, and M. Fleischhauer, *Phys. Rev. Lett.* **125**, 215701 (2020).

[24] Z.-M. Huang and S. Diehl, *Mixed state topological order parameters for symmetry protected fermion matter* (2024), arXiv:2401.10993 [cond-mat.quant-gas].

[25] B. Zeng, X. Chen, D.-L. Zhou, and X.-G. Wen, *Quantum information meets quantum matter – from quantum entanglement to topological phase in many-body systems* (2018), arXiv:1508.02595 [cond-mat.str-el].

[26] J. Chen, Z. Ji, C.-K. Li, Y.-T. Poon, Y. Shen, N. Yu, B. Zeng, and D. Zhou, *New Journal of Physics* **17**, 083019 (2015).

[27] S. V. Isakov, M. B. Hastings, and R. G. Melko, *Nature Physics* **7**, 772–775 (2011).

[28] H.-C. Jiang, Z. Wang, and L. Balents, *Nature Physics* **8**, 902–905 (2012).

[29] A. Kitaev and J. Preskill, *Phys. Rev. Lett.* **96**, 110404 (2006).

[30] M. Levin and X.-G. Wen, *Phys. Rev. Lett.* **96**, 110405 (2006).

[31] P. Fromholz, G. Magnifico, V. Vitale, T. Mendes-Santos, and M. Dalmonte, *Phys. Rev. B* **101**, 085136 (2020).

[32] T. Micallo, V. Vitale, M. Dalmonte, and P. Fromholz, *SciPost Physics Core* **3**, 10.21468/scipostphyscore.3.2.012 (2020).

[33] S. Mondal, D. Sen, and A. Dutta, *Journal of Physics: Condensed Matter* **35**, 085601 (2022).

[34] G. Torre, J. Odavić, P. Fromholz, S. M. Giampaolo, and F. Franchini, *Long-range entanglement and topological excitations* (2023), arXiv:2310.16091 [cond-mat.str-el].

[35] A. Arora, A. Kejriwal, and B. Muralidharan, *On the conclusive detection of majorana zero modes: conductance spectroscopy, disconnected entanglement entropy and the fermion parity noise* (2023), arXiv:2303.03837 [cond-mat.mes-hall].

[36] H. Pichler, G. Zhu, A. Seif, P. Zoller, and M. Hafezi, *Phys. Rev. X* **6**, 041033 (2016).

[37] A. Elben, B. Vermersch, M. Dalmonte, J. I. Cirac, and P. Zoller, *Phys. Rev. Lett.* **120**, 050406 (2018).

[38] T. Brydges, A. Elben, P. Jurcevic, B. Vermersch, C. Maier, B. P. Lanyon, P. Zoller, R. Blatt, and C. F. Roos, *Science* **364**, 260 (2019), <https://www.science.org/doi/pdf/10.1126/science.aau4963>.

[39] W. P. Su, J. R. Schrieffer, and A. J. Heeger, *Phys. Rev. Lett.* **42**, 1698 (1979).

[40] W. P. Su, J. R. Schrieffer, and A. J. Heeger, *Phys. Rev. B* **22**, 2099 (1980).

[41] M. Z. Hasan and C. L. Kane, *Reviews of Modern Physics* **82**, 3045–3067 (2010).

[42] X.-L. Qi and S.-C. Zhang, *Reviews of Modern Physics* **83**, 1057–1110 (2011).

[43] G. Lindblad, *Communications in Mathematical Physics* **48**, 119 (1976).

[44] H. P. Breuer and F. Petruccione, *The theory of open quantum systems* (Oxford University Press, Great Clarendon Street, 2002).

[45] J. K. Asbóth, L. Oroszlány, and A. Pályi, *A Short Course on Topological Insulators* (Springer International Publishing, 2016).

[46] D. S. Simon, S. Osawa, and A. V. Sergienko, *Journal of Physics: Condensed Matter* **31**, 045001 (2018).

[47] M. V. Berry, *Proceedings of the Royal Society of London. A. Mathematical and Physical Sciences* **392**, 45 (1984).

[48] J. Zak, *Phys. Rev. Lett.* **62**, 2747 (1989).

[49] H. Schomerus, *Opt. Lett.* **38**, 1912 (2013).

[50] S. Weimann, M. Kremer, Y. Plotnik, Y. Lumer, S. Nolte, K. G. Makris, M. Segev, M. C. Rechtsman, and A. Szameit, *Nature materials* **16** 4, 433 (2017).

[51] H. Carmichael, *Statistical Methods in Quantum Optics 1: Master Equations and Fokker-Planck Equations*, Theoretical and Mathematical Physics (Springer Berlin Heidelberg, 2013).

[52] A. J. Daley, *Advances in Physics* **63**, 77–149 (2014).

[53] M. B. Plenio and P. L. Knight, *Reviews of Modern Physics* **70**, 101–144 (1998).

[54] K. Mølmer, Y. Castin, and J. Dalibard, *J. Opt. Soc. Am. B* **10**, 524 (1993).

[55] K. W. Yip, T. Albash, and D. A. Lidar, *Physical Review A* **97**, 10.1103/physreva.97.022116 (2018).

[56] Y. L. Gal, X. Turkeshi, and M. Schirò, *Entanglement dynamics in monitored systems and the role of quantum jumps* (2024), arXiv:2312.13419 [cond-mat.stat-mech].

[57] W. Verstraelen and M. Wouters, *Applied Sciences* **8**, 1427 (2018).

[58] Rényi entropy has also been proven suitable for the definition of the DEE [31, 32], even though its first definition has been given using the von Neumann entanglement entropy.

[59] S^D is not unique: other combinations could also work as detectors, but with less experimental relevance and a more complicated interpretation in terms of mutual information [31].

[60] I. Peschel, *Journal of Physics A: Mathematical and General* **36**, L205 (2003).

[61] On the other hand, by considering the SBD jump operators of Eq. (4), the equation for \mathbf{G} is of the form

$$\dot{\mathbf{G}} = -i[\mathbf{H}_{\text{SSH}}, \mathbf{G}] - \frac{\gamma}{2} \left\{ 4\mathbf{G} + e^{i\theta} (\mathbf{G}_\uparrow + \mathbf{G}_\rightarrow) + e^{-i\theta} (\mathbf{G}_\downarrow + \mathbf{G}_\leftarrow) - \mathbf{G}(\mathbf{1}_0 + \mathbf{1}_{N-1}) - (\mathbf{1}_0 + \mathbf{1}_{N-1})\mathbf{G} \right\},$$

where $\mathbf{1}_i$ is the matrix with a single nonzero element equal to 1 at the i -th place along the diagonal, $\mathbf{G}_\uparrow, \mathbf{G}_\downarrow, \mathbf{G}_\rightarrow, \mathbf{G}_\leftarrow$ are matrices with a cyclic shift on rows (columns) so that the first or last row (column), respectively, is replaced by zero entries. In this case of global SBD dynamics, $G_{1,L}$ varies in the same way as under the global SPD dynamics of Fig. 3. The results related to the SBD case are equivalent to those plotted in the main text.

[62] Y. Le Gal, X. Turkeshi, and M. Schirò, *SciPost Physics* **14**, 10.21468/scipostphys.14.5.138 (2023).

[63] D. Wang, S. Xu, Y. Wang, and C. Wu, *Phys. Rev. B* **91**, 115118 (2015).

[64] G. B. Mbeng, A. Russomanno, and G. E. Santoro, *SciPost Physics Lecture Notes* **10.21468/scipostphyslectnotes.82** (2024).

[65] The standard definition by Kitaev, which in row-vector form would read:

$$\begin{aligned} \check{\mathbf{c}} &= (\check{c}_1, \check{c}_2, \check{c}_3, \check{c}_4, \dots, \check{c}_{2N-1}, \check{c}_{2L})^T \equiv \\ &\equiv (\check{c}_{1,1}, \check{c}_{2,1}, \check{c}_{1,2}, \check{c}_{2,2}, \dots, \check{c}_{1,N}, \check{c}_{2,L})^T, \end{aligned} \quad (\text{F10})$$

mixes the different blocks of the Nambu fermions in a way that makes the algebra more complicated.

- [66] T. Prosen, *Journal of Statistical Mechanics: Theory and Experiment* **2010**, P07020 (2010).
- [67] T. Prosen, *New Journal of Physics* **10**, 043026 (2008).
- [68] A. Kitaev, V. Lebedev, and M. Feigel'man, in *AIP Conference Proceedings* (AIP, 2009).
- [69] C.-K. Chiu, J. C. Teo, A. P. Schnyder, and S. Ryu, *Reviews of Modern Physics* **88**, [10.1103/revmodphys.88.035005](https://doi.org/10.1103/revmodphys.88.035005) (2016).
- [70] J. Surace and L. Tagliacozzo, *SciPost Physics Lecture Notes* [10.21468/scipostphyslectnotes.54](https://doi.org/10.21468/scipostphyslectnotes.54) (2022).
- [71] L. M. Sieberer, M. Buchhold, J. Marino, and S. Diehl, *Universality in driven open quantum matter* (2023), [arXiv:2312.03073 \[cond-mat.stat-mech\]](https://arxiv.org/abs/2312.03073).
- [72] G. Passarelli, V. Cataudella, and P. Lucignano, *Physical Review B* **100**, [10.1103/physrevb.100.024302](https://doi.org/10.1103/physrevb.100.024302) (2019).
- [73] N. Friis, *New Journal of Physics* **18**, 033014 (2016).
- [74] N. Friis, A. R. Lee, and D. E. Bruschi, *Physical Review A* **87**, [10.1103/physreva.87.022338](https://doi.org/10.1103/physreva.87.022338) (2013).